Chemical Engineering Science 287 (2024) 119763

Contents lists available at ScienceDirect

Chemical Engineering Science

journal homepage: www.elsevier.com/locate/ces

Multi-objective optimization of heat exchanger network with disturbances based on graph theory and decoupling

Zixuan Zhang [a], Liwen Zhao [a], Ibrahim Tera [a], Guilian Liu [a,b,*]

[a] School of Chemical Engineering and Technology, Xi'an Jiaotong University, Xi'an 710049 Shaanxi, China
[b] Engineering Research Center of New Energy System Engineering and Equipment, University of Shaanxi Province, Xi'an Shaanxi 710049, China

ARTICLE INFO

Keywords:
Disturbance
Decoupling
Excitation
Graph theory
Heat exchanger network
Multi-objective optimization

ABSTRACT

Disturbance poses a significant challenge to highly coupled chemical systems. In this work, a multi-objective optimization framework is developed for reducing the impact of fluctuations on heat exchange networks (HENs) based on graph theory and decoupling. The framework bridges the gap between algebra and structure of HEN through a directed graph (Digraph) and defines the Excitation as a fluctuation impact indicator. The Non-dominated Sorting Genetic Algorithm II (NSGA-II) is improved for generating feasible solutions and global optimality, and the quasi-gradient is applied to select an equilibrium solution from the Pareto Front. Two case studies are conducted, and the equilibrium solution is selected based on quasi-gradient. For the literature case, the Excitation of the equilibrium solution and the total annual cost is reduced by 56.15% and 2.12%, respectively. For the coal-to-methanol system, the utility consumption and Excitation are 29.6% and 264.50% lower than the results of the Aspen Energy Analyzer, respectively.

1. Introduction

The chemical industry is one of the key sectors of the national economy. It consumes a large amount of resources and generates a variety of pollutants. More than 50 % of the chemical industry's direct emissions come from the combustion of fossil fuels. Today, the industry faces two challenges, namely the continued development of the sector and the reduction of carbon emissions (Chew et al., 2023). To achieve carbon neutrality, chemical companies need to keep energy and raw material consumption to a minimum level and maximize the device's operational efficiency and production flexibility (Nair et al., 2023).

The chemical production process comprises reactors, separators, heat exchanger networks (HENs), and utilities. The reactors and separators influence the HEN, as their feeds and products are generally the hot and cold streams of HEN. Disturbances of reactors and separators, such as catalyst deactivation, equipment failure, human-made faults, and extreme weather, induce the HEN's uncertainties. The disturbance and uncertainty affect the optimal match between hot and cold streams, the HEN's minimum utility consumption, and the production's safety and stability. Hence, optimizing HEN with disturbance and uncertainty should be given more attention.

Since the 1980 s, scholars have developed multiple thermodynamic and mathematical programming methods to design and optimize HEN. The pinch technology is the most influential among them and has been widely used to synthesize HEN (Linnhoff and Hindmarsh, 1983). The mathematical programming methods can automatically target a HEN with the minimum annualized cost, no matter the problem's complexity. Some of these mathematical programming methods are widely used, including the mixed integer linear programming (MILP) methods based on the transshipment model (Papoulias and Grossmann, 1983), the mixed integer nonlinear programming (MINLP) transshipment model proposed by Floudas et al. (1986), and the superstructure model (Yee et al., 1990).

Scholars analyzed the impact of uncertain parameters on utility consumption (Charnkhuang et al., 2020; Lee et al., 2021), considering different units and their coupling with HEN. Hafizan et al. (2019) established a mathematical model for minimizing costs, with the supply temperature fluctuations, heat exchanger size, bypass location, and economic performance considered. Ryu et al. (2020) proposed a generalized framework for formulating superstructure-based optimization models for holistic process synthesis. Zhang et al. (2020) combined the pinch and mathematical programming methods and proposed an integration approach for the reactor-distillation column-recycle-HEN system. Zhu et al. (2020) developed a stochastic programming model for cooling water systems based on the approximation of multivariate

* Corresponding author.
E-mail addresses: guilianliui@mail.xjtu.edu.cn, guilianliui@mail.xjtu.edu.cn (G. Liu).

https://doi.org/10.1016/j.ces.2024.119763
Received 25 August 2023; Received in revised form 10 January 2024; Accepted 13 January 2024
Available online 18 January 2024

Nomenclature

Area	Heat transfer area, m^2
area	Heat transfer area, m^2
A, B	Any real number
CM	Medium cost of utilities, $\$\cdot kg^{-1}$
$COST_{fixed}$	Annualized fixed cost of the heat exchanger, $\$\cdot y^{-1}$
$COST_{investment}$	Annualized investment cost of the heat exchanger, $\$\cdot y^{-1}$
$COST_{total}$	Annualized total cost, $\$\cdot y^{-1}$
$COST_{utility}$	Annualized utility consumption cost, $\$\cdot y^{-1}$
Cp, CP	Heat capacity of streams, $kW\cdot h\cdot kg^{-1}\cdot{}^{\circ}C^{-1}$
CpM	Heat capacity or latent heat of the medium, $kJ\cdot{}^{\circ}C^{-1}\cdot kg^{-1}$
d	Decision variables
Distance	Distance from actual solution to theoretical optimal solution
Energy	Energy objective, kW
Eq	Set of equations of all heat transfer units
$Eq_{balance}$	Heat balance equation
$Eq_{transfer}$	Heat transfer equation
Excitation	Excitation objective
F	Flow rate, $kg\cdot h^{-1}$
Hour	Annual operating time of the heat exchanger, $h\cdot y^{-1}$
H(i)	Number of fluctuation transmission paths of stream *i*
Incidence	Incidence matrix of directed graph
K	Total heat transfer coefficient, $kW\cdot m^{-2}\cdot{}^{\circ}C^{-1}$
LMTD	Logarithmic mean heat exchange temperature difference, °C
L(j)	Number of heat exchangers of path *j*
N_C	Set of cold streams
N_H	Set of hot streams
N_S	Set of stages
n, m,i	Dimensions
obj	Objectives of multi-objective optimization model
P	number of the streams
pop	Entire population
Q	Heat exchange load, kW
QG	The quasi-gradient of points in Pareto Front
QU	Heat load of the utility heat exchanger, kW
rank	Solution set with the same dominance level
s	State variables
SC_D^S	First-order sensitivity coefficient matrix of the state variable vector relative to the decision variable vector
$Sensitivity_d^s$	First-order sensitivity of the state variable relative to the decision variable
S, D	State variable vector and decision variable vector
s^*, d^*	Stable value of the variable
T	Temperature of streams, °C
t	Temperature of stages, °C
Year	Depreciation years of heat exchanger, y
Z	Binary (0–1) variables representing the existence of heat exchangers
γ	Utility cost coefficient, $\$\cdot kJ^{-1}$
$\Delta s, \Delta d$	Magnitude of variable change
ΔT	Temperature difference between the inlet and outlet medium, °C
Δt_{min}	Minimum heat exchange temperature difference, °C

Subscripts

C	Cold streams
CU	Cooling utilities
H	Hot streams
HU	Heating utilities
in	Inlet
max	Maximum
min	Minimum
out	Outlet
S	Stages

Superscripts

in	Inlet
out	Outlet

Abbreviation

DFS	Depth-First Search
Digraph	Directed graph
HEN	Heat exchanger network
MILP	Mixed integer linear programming
MINLP	Mixed integer nonlinear programming
No.	Number
NSGA-II	Non-dominated Sorting Genetic Algorithm II

probability distribution. Mohanan and Jogwar (2022) utilized a new energy allocation method to control the transmission path of disturbances, thereby reducing the impact of disturbances on utility consumption. Zhao and Liu (2023) developed bottleneck identification and debottlenecking strategies based on topology analysis for HEN with disturbances. However, the coupling between different units significantly increases the model's complexity, raising the computational cost and bringing challenges to the process system's stable production.

Multiple sensitivity analysis models were developed to study the influence of fluctuations on the HENs and are suitable for both linear and nonlinear parameter relations. The sensitivity method developed based on HEN's inherent linear characteristics (Ratnam and Patwardhan, 1991) has high calculation efficiency and can be applied to cases with multiple and significant parameter variations. Jiang et al. (2014) evaluated the HEN's flexibility and retrofitted the HEN by strengthening the most sensitive heat exchanger and avoiding the addition of new equipment. Li et al. (2015) constructed a direction matrix to describe the deviation of uncertain parameters and proposed a subnetting decoupling strategy for large-scale and non-convex problems. The proposed method is proven to be efficient. Sensitivity analysis has been widely used in operation units but is rarely carried out in designing HENs with resistance to fluctuations. Cardoso-Fernández et al. (2023) proposed a method with an artificial intelligence model for global sensitivity analysis of a generator-absorber heat exchange system's thermal performance with a hybrid energy source.

Flexible HEN is an elegant way to handle parameter fluctuations. It was first proposed in the 1980 s (Grossmann et al., 1983; Morari, 1983), together with the index for operational flexibility (Swaney and Grossmann, 1985a, 1985b). Calandranis and Stephanopoulos (1986) proposed a designer-driven method to analyze the operability of HENs. The flexible HENs, considering the temperature, flow rate, and heat capacity variations, were developed in the 1990 s (Aguilera and Nasini, 1995; Cerda et al., 1990; Cerda and Galli, 1990; Galli and Cerda, 1991). Galli and Cerda (1998); Galli and Cerdá (2001) took the topological location of the heat exchanger in the process into consideration. In recent studies, multi-period flexible HENs (Kang and Liu, 2018a, 2018b; Miranda et al., 2016; Verheyen and Zhang, 2006) and large-scale parameter variations (Li et al., 2015; Payet et al., 2018; Pintaric and Kravanja, 2015; Zirngast et al., 2021) have been the hot research topics. Based on fuzzy game theory, Tian and Li (2023) determined the contribution of each plant when the decision-making environment is uncertain and optimized the inter-plant HEN under uncertain flow. However, enhancing HEN's

flexibility will increase the investment cost because of a larger heat transfer area. And it also cannot provide a feasible solution when the operating margin is exceeded. In the references introduced above, the influence of parameter fluctuations regarding the sensitivity and operational flexibility of HEN has been analyzed, while the impact of HEN's topology on parameter fluctuations was not investigated.

Based on the complex HEN's topology, a method was developed to constrain the size of the feasible region and successfully solve the problem of "combination explosion" (Wang et al., 1999). Zhu et al. (1996) proposed a method to identify load loops and downstream paths based on spanning trees. Gu and Vassiliadis (2014) demonstrated that Euler's formula cannot always be applied to pinch technology. In the design of a heat recovery network, the minimum number of matches (Bagajewicz and Valtinson, 2014; Letsios et al., 2018) is also associated with graph theory. Kang et al. (2016) reconstructed the hierarchical clustering in the context of graph theory, optimized the structural coupling between control and operational variables, and successfully applied it to synthesizing fuel cell systems and HENs. Although the above studies have combined graph theory with HEN optimization, no research has employed graph theory to analyze the influence of parameter fluctuations. The Digraph (directed graph) has not been reported for HEN synthesis.

According to an open literature survey, most studies on the synthesis of HEN with disturbances focus on the trade-off between the HEN's operational flexibility and annual total cost, while the mechanism of fluctuation transmission and its impact remains unclear; the topology structure of the HEN was not studied from the decoupling perspective, which can minimize the fluctuation transmission in the system with the aid of graph theory. Besides, decoupling is not always a win–win situation; it also increases utility consumption, and therefore, it is necessary to adopt multi-objective optimization methods.

The main methods to solve multi-objective problems include the simple additive weighting method, the ε-constraint method (Haimes et al., 1971), and the Pareto method (Pareto, 1955). Multi-objective optimization based on the Pareto method has been widely used in applied mathematics and engineering, and the classical algorithms include multi-objective genetic algorithm (Coello Coello and Christiansen, 1995; Fonseca and Fleming, 1995), ant colony algorithm (Gambardella and Dorigo, 1996), and multi-objective particle swarm algorithm (Moore et al., 2000). For chemical process systems, multi-objective optimization is often used to trade off economy and environment (Pavão et al., 2017; Ravagnani et al., 2014; Xu et al., 2023; Yang et al., 2023), economy and consumption (Toffolo (2009a); Yang et al., 2020), as well as economy and system characteristics (Francesconi et al., 2017; Lee et al., 2020; Lv et al., 2017; Stampfli et al., 2023). Unfortunately, the above multi-objective optimization studies do not pay attention to the uncertainty of system parameters.

This study aims to establish a multi-objective optimization model for HEN with disturbances. The Digraph will be employed to describe the parameter fluctuations and topological structure of HEN. An evaluation model will be built to analyze the impact of parameter fluctuations. The multi-objective optimization model is constructed to minimize the HEN's utility consumption and decoupling degree (Excitation) and solved by the improved Non-dominated Sorting Genetic Algorithm II (NSGA-II). The quasi-gradient will be applied to select an equilibrium solution from the Pareto Front. Two cases will be studied to demonstrate the rationality of the proposed model.

2. Problem description and challenges

Various factors, such as catalyst activity, extreme weather, equipment failures, and manual operations, can lead to the uncertainty of the chemical process. To ensure the system's stable operation under uncertainty, engineers usually leave a certain design margin for the operating unit, while the wider margin will increase investment costs. Generally, it is necessary to design the devices with suitable margins while improving the system's adaptability to uncertain factors through other measures.

In a chemical process, units or devices affect each other. For example, in Fig. 1 (a), the reactor's outlet stream is used in the distillation column's reboiler to provide energy, and the two devices are coupled. In Fig. 1(b), the reactor's outlet stream and the distillation column's reboiler are cooled and heated by utilities, and the reactor and distillation column are decoupled. When the temperature of the reactor's outlet stream changes due to factors such as catalyst deactivation, the performance of the distillation column shown in Fig. 1(a) will be affected, while the distillation column shown in Fig. 1(b) will not. Hence, decoupling the devices can reduce the influence of uncertain parameters. However, the energy consumption and operating costs will increase. Decoupling the units or devices and targeting the suitable fewer devices to enhance instead of all is crucial. Thus, the investment costs can be reduced, and the system's ability to resist fluctuations is enhanced.

The hot and cold streams in the HEN couple through the heat exchanger. Excessive or unreasonable coupling will increase the system's complexity and have a negative effect on the system's stability. It is necessary to decouple the HEN to enhance the ability to resist fluctuations. On the other hand, decoupling the HEN will increase utility consumption. There are two main challenges in designing a HEN with low utility costs and resistance to parameter fluctuations. One is to develop a reasonable model to measure the decoupling degree of units; the other is to design a multi-objective optimization algorithm to trade off coupling and decoupling and enhance the HEN's ability to resist parameter fluctuations with less utility increment.

This study aims to figure out how to design a HEN with low coupling while ensuring that the utility consumption increases slightly and establish an improved superstructure model with the energy consumption and the disturbance resistance both considered. The Excitation, defined as the fluctuation degree of the whole network excited by the parameter changes, is put forward to measure the decoupling between units, i.e., the ability to resist fluctuations. Since the parameter fluctuation is related to the topological structure between units, the graph theory will be applied to transform the HEN into the Digraph and improve the NSGA-II with decapitation disaster, population migration, and gene pool strategies. Based on the idea of greed and dynamic programming, forbidden matching and maximum energy matching strategies will be introduced to transform the constraints and improve the quality of the initial solution. The effectiveness and feasibility of the model will be verified through comparison and analysis. The overall procedure of the proposed method is shown in Fig. 2.

The main hypotheses are:

1) Each stream's target temperature is fixed, and the initial temperature changes within a known range;
2) Only the variation of one parameter is considered for each stream;
3) Parameter fluctuations instantaneously propagate along downstream paths (Linnhoff and Kotjabasakis, 1986; Zhu et al., 1996) without backpropagation;
4) Isothermal mixing and the superstructure model without stream splitting are adopted.

3. Directed graph (Digraph) of HEN

3.1. Transformation of HEN to Digraph

The grid diagram shown in Fig. 3 is widely employed to illustrate the HENs. A vertical line joining two heat exchangers (denoted by E) on the two streams represents a heat exchange match. HE indicates the heater consuming heating utility, while CE stands for the cooler using the cooling utility. This diagram can clearly distinguish whether there is a heat exchange between streams and the order of heat exchange, while it cannot show a HEN's actual topology, which means it is unable to

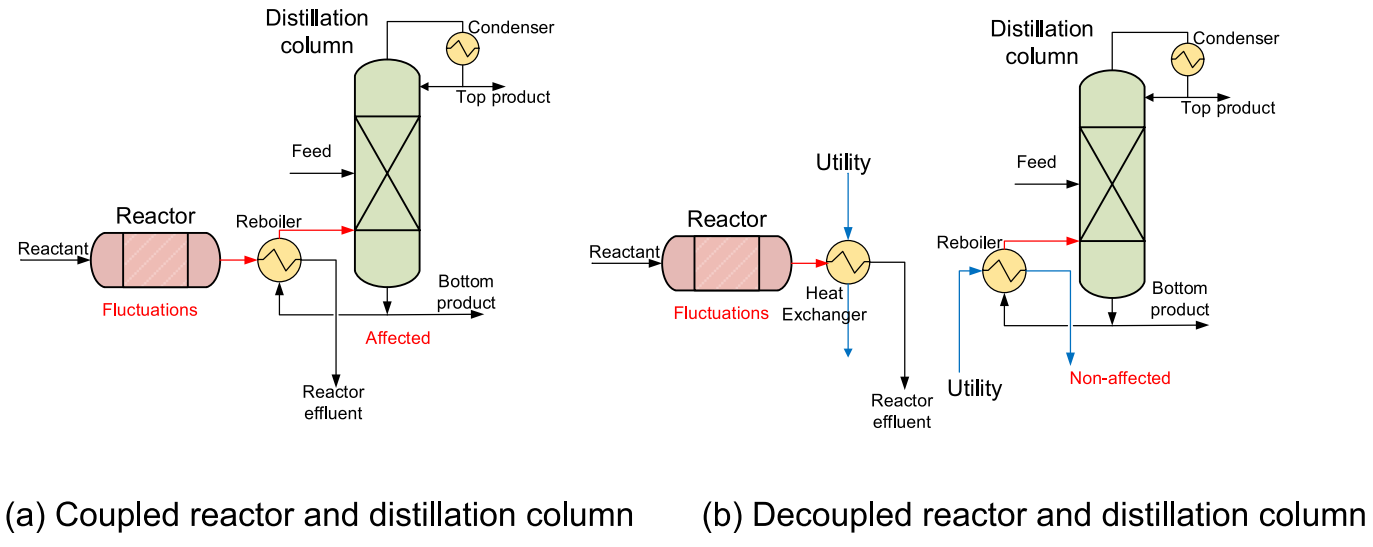

Fig.1. Coupling and decoupling relationship between units.

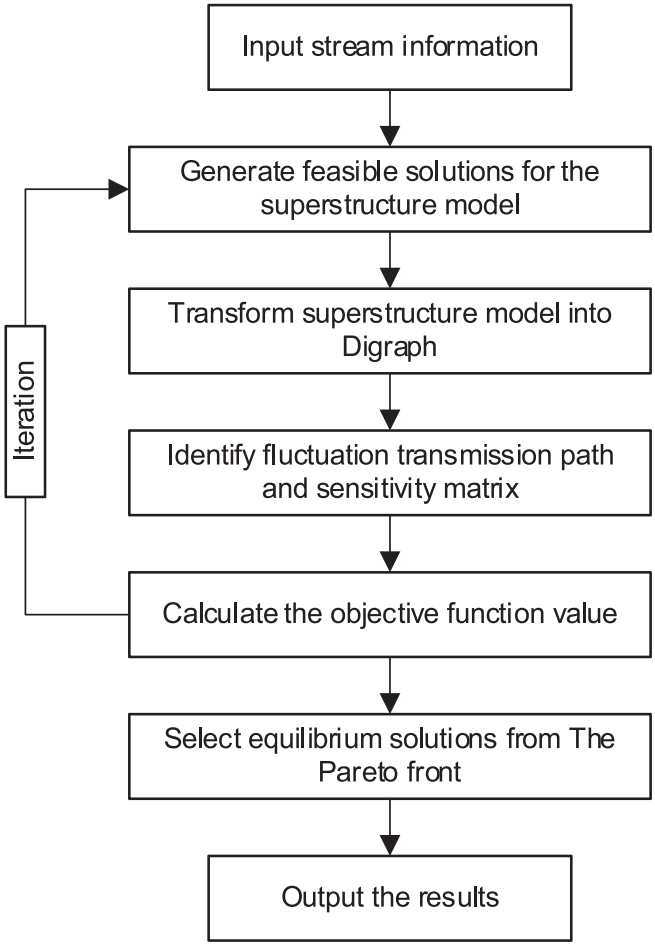

Fig.2. Overall produce of multi-objective optimization of HEN with disturbances.

analyze the transformation of fluctuations through downstream paths (Linnhoff and Kotjabasakis, 1986; Zhu et al., 1996), nor be used in automatic computing.

The Digraph can reflect the topological relationship between units and is widely used in process simulation based on the sequential modular method (Kisala et al., 1987). For the HEN, its characteristics and structure can be represented by the Digraph, i.e., the directed graph, which algebraic matrices can easily represent and hence benefits the storage of the HEN's structure and sensitivity analysis. The HEN's grid diagram can be transferred into a Digraph according to the following rules:

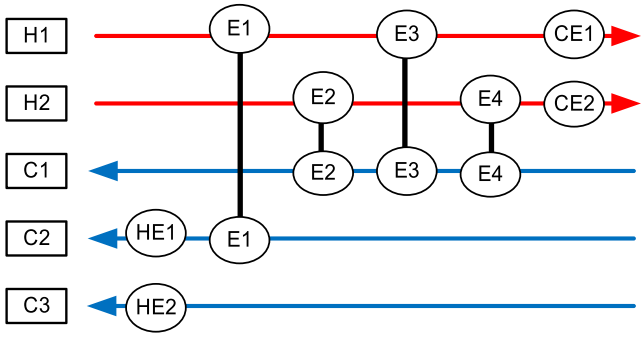

Fig.3. The grid diagram of a five-stream HEN.

1) The initial and target of each stream are taken as virtual nodes, and each virtual node's in-degree or out-degree is only allowed to be 1. The in-degree is the number of directed lines that inlet the node; the out-degree is the number of directed lines leaving the node;
2) Each heat exchanger is taken as a real node; for the real node corresponding to the utility heat exchanger (cooler or heater), both its in-degree and out-degree are 1; for a real node corresponding to the heat exchanger between two streams, both its in-degree and out-degree are 2;
3) If a stream flows between two nodes, a directed line is added according to the stream's flow direction.

Based on these rules, the HEN shown in Fig. 3 can be transformed into a Digraph shown in Fig. 4.

3.2. *Matrices of HEN*

Parameter fluctuations can be directly or indirectly transmitted downstream through the heat exchanger. However, the HEN's structure is usually quite complex, and it is impossible to observe whether there is a path between two heat exchangers.

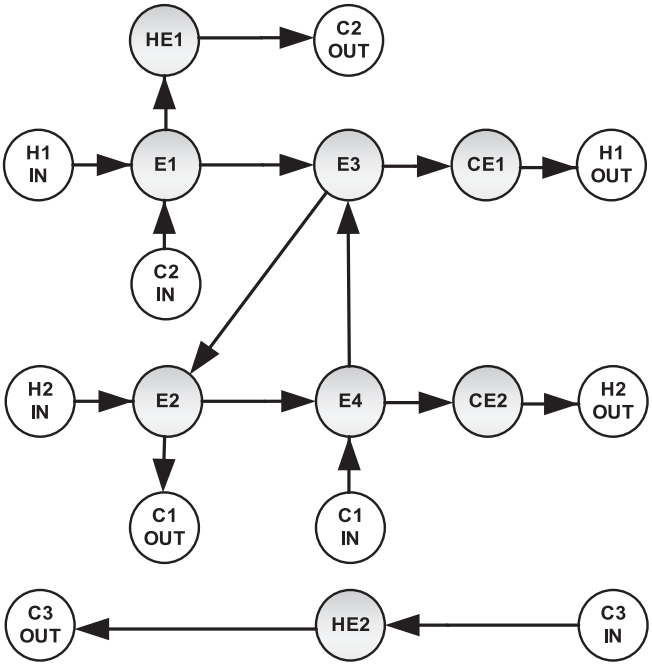

Fig.4. Digraph of the HEN shown in Fig. 3.

The HEN's Digraph can be expressed by the matrix, which is effective and necessary for analyzing the parameter fluctuation with the computer. The Adjacency matrix and Incidence matrix (Deo, 1975), which are suitable for different analysis scenarios, can be employed to store the structural information of nodes and edges. The Reachability matrix (Deo, 1975) can be utilized to determine whether the parameter fluctuation of a stream will be transmitted downstream, and it can be calculated based on the adjacency matrix and the multiplication, power multiplication, Warshall algorithm (Warshall, 1962), or Tarjan algorithm (Tarjan, 1971). The pseudo-code of targeting the Reachability matrix by the multiplication algorithm is shown in Table A1 in Appendix A.

3.3. Irrelevant subsystem

Irrelevant subsystems mean that there is no path for any two points belonging to different subsystems, which are also known as connected components (Chen et al., 2015; Gura et al., 2015).

In the Digraph of the HEN, the edge represents the mass transfer, and the node represents the heat transfer. Subsystems without heat or mass transfer are taken as irrelevant subsystems of HEN. Parameter variations between irrelevant subsystems cannot be transmitted to each other. For an HEN with a certain number of heat exchangers, the more the irrelevant subsystems, the lower the complexity of the whole system, the higher the degree of decoupling, and the less influence the parameter fluctuations (Li et al., 2014a, 2014b).

The degree matrix and Laplace matrix are introduced to identify the HEN's irrelevant subsystems (Akutsu and Tamura, 2012; Kann, 1992; Yan, 2004). For the Digraph shown in Fig. 4, two irrelevant subsystems can be identified, as shown in Fig. 5.

4. Disturbance transmission analysis model

The stream parameters often fluctuate in chemical production due to internal or external interferences. For example, catalyst deactivation can lead to the fluctuation of the reactor's effluent, and weather changes affect the working conditions of the distillation column and the heat exchanger, consequently affecting product quality and energy consumption. Parameter fluctuations are acceptable within a specific range,

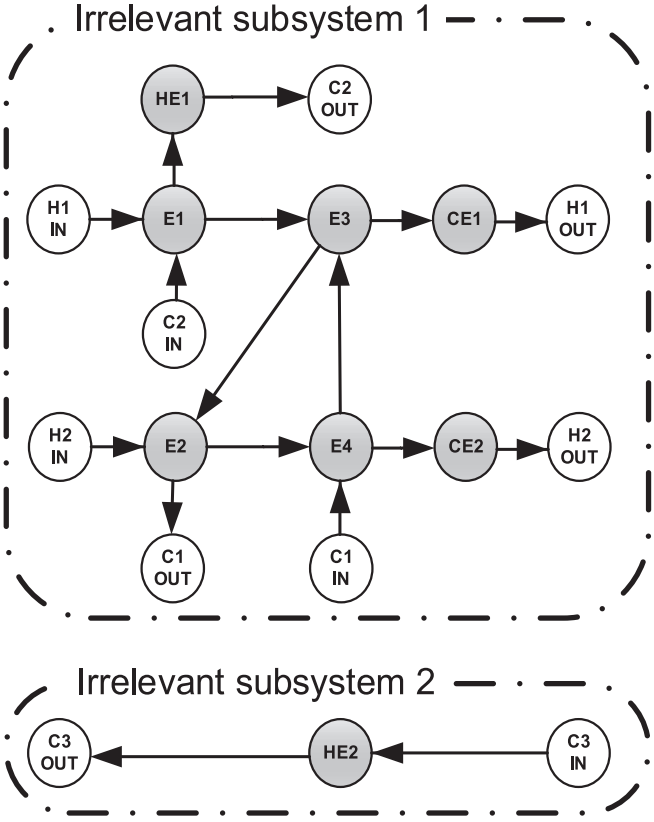

Fig.5. Two irrelevant subsystems of the HEN shown in Fig. 3 and Fig. 4.

but once the design margin is exceeded, they will have a negative impact on the system. For highly coupled systems, parameter fluctuations can be transmitted among devices. It is significant to explore how the parameter fluctuations shift in the HEN and establish a model to evaluate their impact. This section will use adjacency and reachability matrices to determine whether the fluctuation is reachable. A systematic model is established to explore the fluctuation transfer path based on the node information stored in the adjacency matrix.

4.1. Excitation and its calculation

For a highly coupled HEN, the Excitation measures the degree of coupling among heat exchangers and the influence of parameter fluctuations on the system. High Excitation represents a high coupling degree among heat exchangers and impacts the whole system significantly.

4.1.1. Fluctuation transmission path

To explore the parameter fluctuations' influence on the HEN, it is necessary to clarify the fluctuation transmission path first. The fluctuation transmission from the decision variable to the state variable is the fluctuation transmission path (Linnhoff and Kotjabasakis, 1986). The decision variable refers to the variable directly disturbed, and the state variable refers to the variable affected by the decision variables (Yang et al., 1996). Zhao and Liu (2022) defined the path/direction, key equipment, and fluctuation transmission path, and clarified the calculation formula and law of single-variable and multi-variable load migration. The fluctuation transmission path is equivalent to the heat flow path (Kemp, 2007), which refers to the route connecting the heaters and coolers, including all the heat exchangers in the route.

However, in practical chemical systems, the possible paths of load and fluctuation transfer are not single and are limited by the heat transfer area. The model proposed by Zhao and Liu (2022) cannot automatically identify all possible fluctuation transmission paths. This

work will improve this method to identify all possible paths automatically.

The basic rules for targeting all fluctuation transmission paths are as follows:

1) A heat flow path from the fluctuation parameter to a stream's outlet is a potential fluctuation transmission path;
2) The heat flow path can only propagate in the stream's flow direction and cannot propagate reversely;
3) There is no heat load loop in the fluctuation transmission path since the heat load loop always satisfies the node enthalpy balance (Shivakumar and Narasimhan, 2002). In other words, each heat exchanger in a fluctuation transmission path appears only once.

The system shown in Fig. 3 will be an illustrative example for analyzing the fluctuation migration. When the inlet temperature of H1 fluctuates, the fluctuation migration path is shown in Fig. 6.

4.1.2. Global sensitivity

The parameter fluctuation has a different impact on the heat exchangers of the fluctuation transmission path. The sensitivity and sensitivity coefficient are introduced as weights to measure the impact accurately. The sensitivity coefficient reflects the degree of the state variable change with the decision variable. If the state variable is very sensitive to the fluctuation of the decision variable, the sensitivity coefficient would be high, and it is challenging to keep stable operations.

For a system with n decision variables and m state variables, the state and decision variables are represented by s and d, respectively. The first-order sensitivity of the state variable relative to the decision variable is expressed in Eq. (1).

$$Sensitivity_d^s = \frac{\Delta s/s^*}{\Delta d/d^*} = \left(\frac{\Delta s}{\Delta d}\right)_{d^*} / \frac{s^*}{d^*} \tag{1}$$

Where, Δs and Δd represent the magnitude of variable change, s^* and d^* represent the stable value of the variable. When $\Delta d \to 0$, the sensitivity coefficient equals $\left(\frac{\Delta s}{\Delta d}\right)_{d^*}$. The matrix of the multi-dimensional sensitivity coefficient is shown in Eq. (2).

$$SC_D^S = \begin{bmatrix} \frac{\partial s_1}{\partial d_1} & \cdots & \frac{\partial s_n}{\partial d_1} \\ \vdots & \ddots & \vdots \\ \frac{\partial s_m}{\partial d_1} & \cdots & \frac{\partial s_m}{\partial d_n} \end{bmatrix}_{m \times n} \tag{2}$$

Where S and D are the state and the decision vectors, respectively, as shown in Eqs. (3) and (4).

$$\boldsymbol{S} = [\, s_1 \quad s_2 \quad \cdots \quad s_m \,]_m \tag{3}$$

$$\boldsymbol{D} = [\, d_1 \quad d_2 \quad \cdots \quad d_n \,]_n \tag{4}$$

Each heat exchange unit's heat balance and heat transfer are described by Eq. (5) and Eqs. (6)–(7).

$$Eq_{balance} = F_C Cp_C \left(t_C^{out} - t_C^{in}\right) - F_H Cp_H \left(t_H^{in} - t_H^{out}\right) = 0 \tag{5}$$

$$Eq_{transfer} = Q - Area \cdot K \cdot LMTD \tag{6}$$

$$LMTD = \frac{\left(t_H^{in} - t_C^{out}\right) - \left(t_H^{out} - t_C^{in}\right)}{\ln[(t_H^{in} - t_C^{out})/(t_H^{out} - t_C^{in})]} \tag{7}$$

Where F denotes the flow rate, kg·h^{-1}; Cp is the heat capacity of streams, kW·h·kg^{-1}·℃$^{-1}$; Q represents the heat load, kW; K is the total heat transfer coefficient, kW·m^{-2}·℃$^{-1}$; $Area$ is the heat transfer area, m^2; $LMTD$ is the logarithmic mean heat exchange temperature difference, ℃, and can be calculated by Eq. (7); t stands for the stream temperature, ℃ ; superscripts H and C represent the hot and cold streams; superscripts in and out denote the inlet and outlet.

For a HEN with i heat exchange units, there are $2i$ heat balance and heat transfer equations, as shown in Eq. (8). The multi-dimensional sensitivity coefficient matrix can be calculated by Eq. (9).

$$\boldsymbol{Eq} = f(\boldsymbol{S}, \boldsymbol{D})_{2i} = 0 \tag{8}$$

$$\boldsymbol{SC}_{\boldsymbol{D}}^{\boldsymbol{S}} = -\left(\frac{\partial \boldsymbol{Eq}}{\partial \boldsymbol{S}}\right)^{-1} \left(\frac{\partial \boldsymbol{Eq}}{\partial \boldsymbol{D}}\right) \tag{9}$$

Where $\boldsymbol{SC}_{\boldsymbol{D}}^{\boldsymbol{S}}$ denotes the sensitivity coefficient matrix, and $\left(\frac{\partial Eq}{\partial S}\right)^{-1}$ denotes the left inverse matrix of $\left(\frac{\partial Eq}{\partial S}\right)$.

4.1.3. Excitation and its definition

The Excitation on a single stream is the value that measures the impact of individual inlet's fluctuation on the entire system. For each parameter fluctuation, there is at least one transmission path. Assuming that there are P streams and stream i undergoes parameter change, there are a total of $H(i)$ fluctuation transmission paths. For path j, there are $L(j)$ heat exchangers. The sensitivity coefficient of the outlet temperature of heat exchanger k to the inlet temperature of the stream i is $\left|\frac{\partial t_k}{\partial T_i^{in}}\right|$.

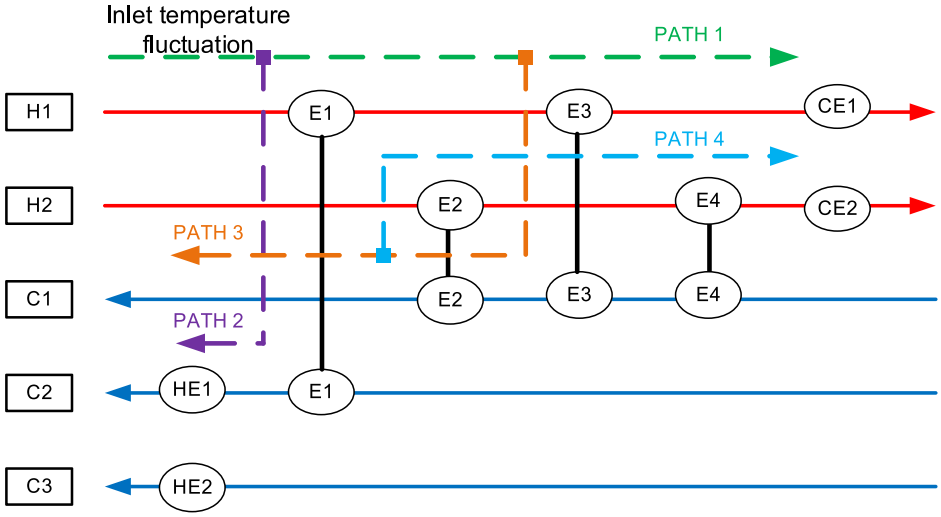

Fig.6. The fluctuation transmission path of the system shown in Fig. 3 when H1′s inlet temperature fluctuates.

For each path j, there is

$$Excitation_{stream_i}^{path_j} = \sum_{k=1}^{L(j)} \left| \frac{\partial t_k}{\partial T_i^{in}} \right| \tag{10}$$

For each stream i, there is

$$Excitation_{stream_i} = \sum_{j=1}^{H(i)} Excitation_{stream_i}^{path_j} \tag{11}$$

And for the whole system, there are

$$Excitation = \sum_{i=1}^{P} Excitation_{stream_i} \tag{12}$$

$$Excitation = \sum_{i=1}^{P} \sum_{j=1}^{H(i)} \sum_{k=1}^{L(j)} \left| \frac{\partial t_k}{\partial T_i^{in}} \right| \tag{13}$$

Based on the structure information stored in the adjacency matrix, Eqs. (5)–(7), Eq. (9), and Eq. (13), the HEN's Excitation can be calculated.

4.2. Algorithm for calculating Excitation

The fluctuation transmission paths shown in the grid diagram can be illustrated in the Digraph. For example, Fig. 6 can be transmitted into Fig. 7. The nodes of all fluctuation transmission paths are in the same independent subsystem. The basic rules for searching all the transmission paths are transformed into the following description in terms of graph theory:

1) All paths from the initial node to the target node are a potential fluctuation transmission path;
2) The path must be connected following the direction of the directed edge; the out-degree and in-degree of the stream's initial node are 1 and 0, respectively, while those of the stream's target node are 0 and 1. For the nodes inside each path, the in-degree and out-degree are 1.
3) Loops do not exist in the path; each node is only accessed once.

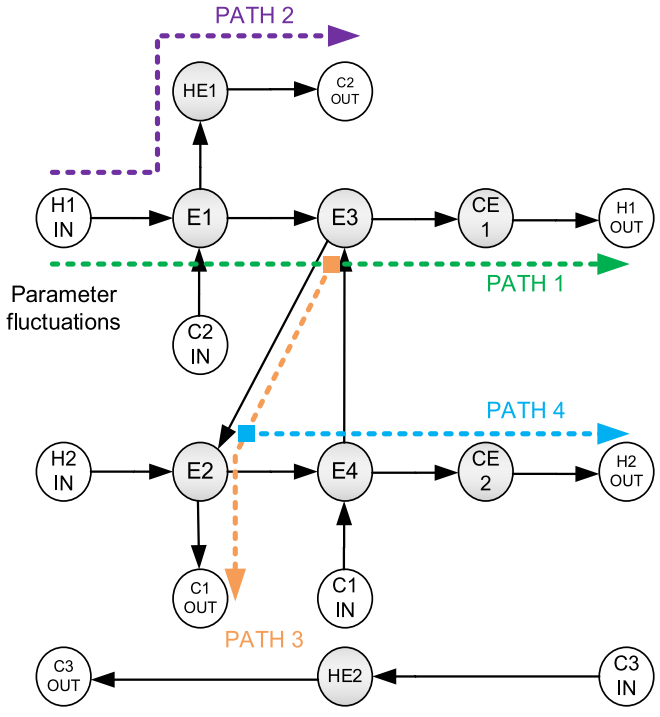

Fig.7. The fluctuation transmission path represented in a directed graph.

Another key to identifying the Excitation is calculating the sensitivity coefficient matrix, whose element is the process equations' partial derivatives over the decision and state variables. In this work, the inlet temperature of each stream is taken as the decision variable, and the outlet temperature of each heat exchanger is the state variable; each heat exchanger's heat load and utilities' inlet/outlet temperatures are constant. The disturbance in flow rate and heat capacity can be discussed by a similar method, and the results are provided in Appendix B.

For any heat exchange unit, the partial derivatives of Eq. (6) over t_H^{in}, t_H^{out}, t_C^{in}, and t_C^{out}, are shown in Eqs. (14)–(17). Table 1 summarizes the partial derivative calculation equations over decision variables and state variables.

$$\frac{\partial Eq_{transfer}}{\partial t_H^{in}} = -KArea/\log\left(\frac{-t_C^{out}+t_H^{in}}{-t_C^{in}+t_H^{out}}\right) + \frac{KArea \times \left(t_C^{in}-t_C^{out}+t_H^{in}-t_H^{out}\right)}{\left(-t_C^{out}+t_H^{in}\right) \times \log\left(\frac{-t_C^{out}+t_H^{in}}{-t_C^{in}+t_H^{out}}\right)^2} \tag{14}$$

$$\frac{\partial Eq_{transfer}}{\partial t_H^{out}} = -KArea/\log\left(\frac{-t_C^{out}+t_H^{in}}{-t_C^{in}+t_H^{out}}\right) - \frac{KArea \times \left(t_C^{in}-t_C^{out}+t_H^{in}-t_H^{out}\right)}{\left(-t_C^{in}+t_H^{out}\right) \times \log\left(\frac{-t_C^{out}+t_H^{in}}{-t_C^{in}+t_H^{out}}\right)^2} \tag{15}$$

$$\frac{\partial Eq_{transfer}}{\partial t_C^{in}} = -KArea/\log\left(\frac{-t_C^{out}+t_H^{in}}{-t_C^{in}+t_H^{out}}\right) + \frac{KArea \times \left(t_C^{in}-t_C^{out}+t_H^{in}-t_H^{out}\right)}{\left(-t_C^{in}+t_H^{out}\right) \times \log\left(\frac{-t_C^{out}+t_H^{in}}{-t_C^{in}+t_H^{out}}\right)^2} \tag{16}$$

$$\frac{\partial Eq_{transfer}}{\partial t_C^{out}} = -KArea/\log\left(\frac{-t_C^{out}+t_H^{in}}{-t_C^{in}+t_H^{out}}\right) - \frac{KArea \times \left(t_C^{in}-t_C^{out}+t_H^{in}-t_H^{out}\right)}{\left(-t_C^{out}+t_H^{in}\right) \times \log\left(\frac{-t_C^{out}+t_H^{in}}{-t_C^{in}+t_H^{out}}\right)^2} \tag{17}$$

The Depth-First Search (DFS) algorithm (Tarjan, 1971), a tool developed for traversing trees or graphs and also having the capacity to explore the branches of the tree as deep as possible, will be employed to search all possible fluctuation transmission paths of the HEN before calculating the Excitation.

Step 1. Input the Initial data. The input data include the stream's temperature, heat capacity flow rate, fluctuation range, utility temperature, etc.

Step 2. Allocate nodes to streams. Assign the nodes and serial numbers to each stream's initial and target, the utility heat exchanger, and the heat exchanger according to the structural information of the feasible solution and the order and flow direction of the stream. The serial number of each node is unique, and each heat exchanger is taken as one node.

Step 3. Search the fluctuation transmission path. The HEN's topological information is stored in the adjacency matrix, and the reachable matrix is calculated according to the pseudo-code shown in Table A1 in Appendix A. Each stream's initial and target are set as the starting and end nodes. If these two nodes are inaccessible, the empty set is output; otherwise, all potential fluctuation transmission paths are searched by the DFS algorithm.

Step 4. Calculate the sensitivity coefficient matrix.

1) Calculate the *KArea* of each heat exchanger according to Eq. (6);
2) Calculate the partial derivative matrix of the process equation vector over the decision variables according to Table 1;
3) Calculate the partial derivative matrix of the process equation vector over the state variables according to Table 1 and Eqs. (14)–(17);
4) Calculate the sensitivity coefficient matrix according to Eq. (9).

Step 5. Calculate the Excitation. Calculate the Excitation of the whole HEN according to the fluctuation transmission path, the sensitivity

Table 1
The partial derivative calculation equations over decision variables and state variables.

	Location of the heat exchange unit	Decision variable	Partial derivative of balance equation				Partial derivative of heat-transfer equation			
			$T_{H,in}$	$T_{H,out}$	$T_{C,in}$	$T_{C,out}$	$T_{H,in}$	$T_{H,out}$	$T_{C,in}$	$T_{C,out}$
$\frac{\partial Eq}{\partial D}$	The first unit in the path	Cold stream's inlet temperature	0	0	$-FCP_C$	0	0	0	Eq.(16)	0
		Hot stream's inlet temperature	FCP_H	0	0	0	Eq.(14)	0	0	0
		The inlet temperature of cold and hot streams	FCP_H	0	$-FCP_C$	0	Eq.(14)	0	Eq.(16)	0
	Not the first unit in the path		0	0	0	0	0	0	0	0
$\frac{\partial Eq}{\partial S}$	The first unit in the path	Cold stream's inlet temperature	FCP_H	FCP_H	0	$-FCP_C$	Eq.(14)	Eq.(15)	0	Eq.(17)
		Hot stream's inlet temperature	0	FCP_H	$-FCP_C$	$-FCP_C$	0	Eq.(15)	Eq.(16)	Eq.(17)
		The inlet temperature of cold and hot streams	0	FCP_H	0	$-FCP_C$	0	Eq.(15)	0	Eq.(17)
	Not the first unit in the path		FCP_H	FCP_H	$-FCP_C$	$-FCP_C$	Eq.(14)	Eq.(15)	Eq.(16)	Eq.(17)

coefficient matrix obtained in the previous steps, and Eq. (13).

Based on the above steps and Eqs. (6) and (9), the Excitation can be automatically calculated and optimized as one of the objectives.

5. Superstructure model for optimizing Excitation and utility consumption

5.1. Multiple-objective superstructure model

The improved superstructure model established in this study is based on the split-less stage-wise superstructure proposed by Yee et al. (1990). For a system with N_H hot streams and N_C cold streams, the number of superstructure's stages (N_S) equals $\max\{N_H,N_C\}$, and the stream mixing is assumed to be isothermal. This superstructure model is a non-convex MINLP problem with multiple locally optimal solutions, and its optimization is challenging.

The Excitation and investment cost generally increase with the number of process stream's heat exchangers while the utility cost decreases. The total cost will decrease first and then increase along with the Excitation, as shown in Fig. 8. Unlike the model proposed by Yee et al. (1990), which adopted the total cost as one of its objectives, this model adopts the energy cost as one of its objectives instead. When the total cost is taken as one of the objectives, the Pareto solution set tends to choose the point with smaller Excitation under the same total cost as the iteration direction, which makes it easily trapped in the local minimizer. Considering the globality, the energy or investment cost is better for iteration. The strategy used in this work to select the equilibrium solution from the Pareto solution set can ensure a lower total cost.

Objectives

$$\min Excitation = \sum_{i=1}^{P}\sum_{j=1}^{H(i)}\sum_{k=1}^{L(j)}\left|\frac{\partial t_k}{\partial T_i^{in}}\right| \tag{18}$$

$$\min Energy = \sum_{i=1}^{N_H} Q_{CU,i} + \sum_{j=1}^{N_C} Q_{HU,j} \tag{19}$$

Constraints.

1) Heat balance of streams

$$\left(T_i^{in} - T_i^{out}\right)\cdot F_i\cdot Cp_i = \sum_{k=1}^{N_S}\sum_{j=1}^{N_C} Q_{i,j,k} + Q_{CU,i} \quad i \in N_H \tag{20}$$

$$\left(T_j^{out} - T_j^{in}\right)\cdot F_j\cdot Cp_j = \sum_{k=1}^{N_S}\sum_{i=1}^{N_H} Q_{i,j,k} + Q_{HU,j} \quad j \in N_C \tag{21}$$

2) Stage-wise superstructure thermal equilibrium

$$\begin{aligned} Q_{i,j,k} &= F_i\cdot Cp_i\cdot\left(t_{i,k}^{in} - t_{i,k}^{out}\right) \\ &= F_j\cdot Cp_j\cdot\left(t_{j,k}^{out} - t_{j,k}^{in}\right) \end{aligned} \quad i \in N_H, j \in N_C, k \in N_S \tag{22}$$

3) Heat balance of heat exchangers

$$Q_{CU,i} = F_i\cdot Cp_i\cdot\left(t_{i,N_S}^{out} - T_i^{out}\right) \quad i \in N_H \tag{23}$$

$$Q_{HU,j} = F_j\cdot Cp_j\cdot\left(T_j^{in} - t_{j,1}^{in}\right) \quad j \in N_C \tag{24}$$

4) Temperature feasibility

$$t_{i,k} \geqslant t_{i,k+1} \quad i \in N_H, k \in N_S - 1 \tag{25}$$

$$t_{j,k} \geqslant t_{j,k+1} \quad j \in N_C, k \in N_S - 1 \tag{26}$$

$$t_{i,N_S}^{out} \geqslant T_i^{out} \quad i \in N_H \tag{27}$$

$$T_j^{out} \geqslant t_{j,1}^{out} \quad j \in N_C \tag{28}$$

5) Heat transfer temperature difference

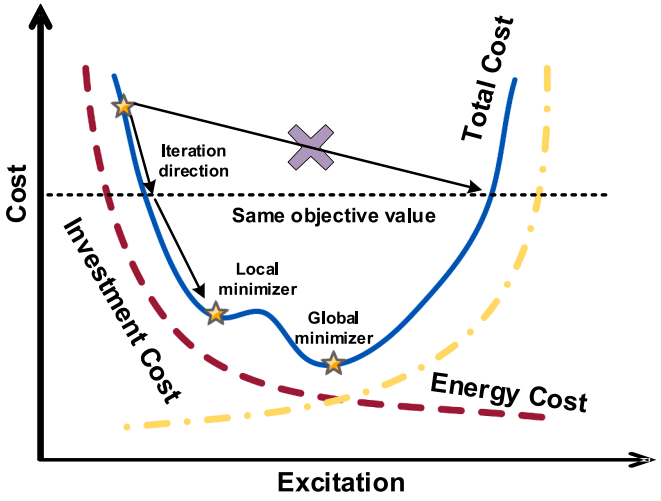

Fig.8. The cost versus Excitation chart.

$$t_{i,k}^{in} - t_{i,k}^{out} \geqslant \Delta t_{\min} \quad i \in N_H, j \in N_C, k \in N_S \tag{29}$$

$$t_{i,k}^{out} - t_{j,k}^{in} \geqslant \Delta t_{\min} \quad i \in N_H, j \in N_C, k \in N_S \tag{30}$$

6) Number of heat exchangers

$$\sum_{i=1}^{N_H} Z_{i,j,k} \leqslant 1 \quad j \in N_C, k \in N_S \tag{31}$$

$$\sum_{j=1}^{N_C} Z_{i,j,k} \leqslant 1 \quad i \in N_H, k \in N_S \tag{32}$$

7) Binary constraint

$$Z_{i,j,k} = \begin{cases} 0 & \text{No heat transfer between streams } i \text{ and } j \text{ in stage } k \\ 1 & \text{Heat transfer exsists between streams } i \text{ and } j \text{ in stage } k \end{cases} \quad i \in N_H, j \in N_C, k \in N_S \tag{33}$$

Where T represents the stream temperature, ℃; t is the stage temperature, ℃; F is the flow rate, kg·h^{-1}; Cp stands for the heat capacity of streams, kW·h·kg^{-1}·℃$^{-1}$; Q is the heat load, kW; Z denotes a binary (0–1) variable, indicating whether the heat exchanger exists or not. Subscripts H and C represent the hot and cold streams, S represents the stage of the superstructure model, and subscripts CU and HU denote the cooling and heating utilities. Superscripts *in* and *out* stand for the inlet and outlet.

This model takes Excitation and utility consumption as optimization objectives. With the structure and energy consumption optimized, the obtained HEN will have strong resistance to parameter fluctuations and low energy consumption.

5.2. Improved NSGA-II algorithm

The traditional multi-objective optimization algorithm generally converts multiple objective functions into one function by a relatively reasonable model. For the optimization in terms of Excitation and utility consumption, there is no clear mathematical relationship between the decision variable and the Excitation, and it is not easy to find a reasonable model to combine two objective functions into one. Hence, the traditional optimization algorithm cannot be used.

NSGA-II (Deb et al., 2002) is an extraordinary multi-objective optimization algorithm and will be improved to optimize the proposed multi-objective MINLP model.

5.2.1. Basic NSGA-II algorithm

The basic NSGA-II includes five steps (Deb et al., 2002).

Step 1. Generate the initial population.

Step 2. Selection, crossover, and mutation. Take roulette and binary championships as selection strategies. Set the probability of mutation in the offspring as 0.5.

Step 3. Elite solution strategy. The top 50 % are selected as the parents of the next generation.

Step 4. Other operator improvement strategies. Implement the population migration and gene pool strategies and trigger the decapitation and disaster strategies under appropriate conditions. The specific descriptions will be introduced in Section 5.2.3.

Step 5. Iteration and convergence. Repeat Steps 2–4 until the number of iterations or convergence conditions is satisfied.

NSGA-II has the following advantages:

1) It does not require a precise mathematical relationship between the objective functions and the decision variables;
2) There is no limitation on linearity, convexity, and continuity of the problem, and thus, it can deal with highly complex models and constraints;
3) Multiple objectives do not need to be converted into one, and the solution can be evaluated based on the non-dominated rank and crowding distance.
4) The data structure of the decision variable ($Z_{i,j,k}$) is suitable for the NSGA-II algorithm's binary coding, crossover, and mutation.

5.2.2. Strategies for generating feasible solutions

Since the HEN's superstructure model has extremely harsh constraints, the randomly generated initial solution is generally infeasible and cannot lead to optimal solutions. Strategies are proposed and employed to ensure that sufficient feasible initial solutions can be generated.

5.2.2.1. Forbidden matching strategy. In the superstructure model, there are three possible temperature relationships between two streams, as shown in Fig. 9. In Fig. 9(a), the T-H line of the hot stream lies above that of the cold stream; the hot and cold streams conform to the temperature constraints and can exchange heat. In Fig. 9(b), the two T-H lines intersect, the two streams partly meet the temperature constraints, and the heat exchange in the temperature interval above the intersecting point is feasible. In Fig. 9(c), the T-H line of the cold stream lies above that of the hot stream, and their match is forbidden, that is, $Z_{i,j,k}$ equals 0, and the corresponding match can be prohibited to improve the

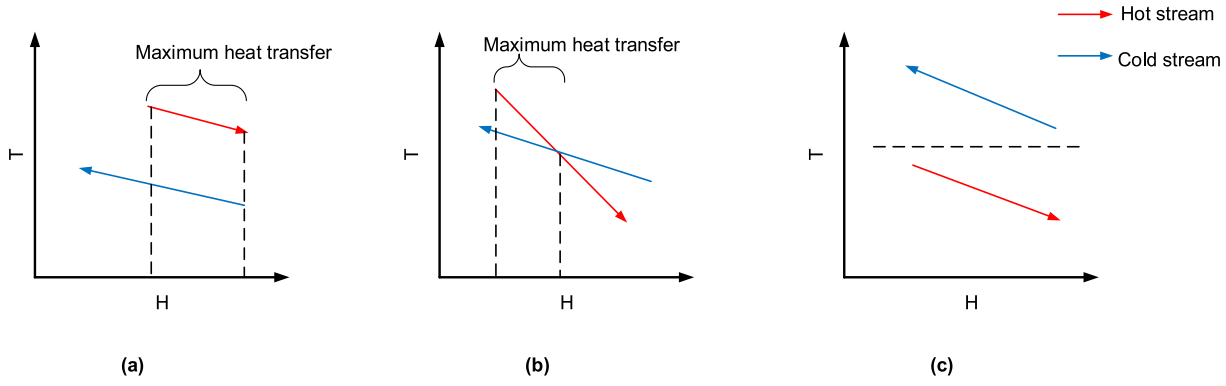

Fig.9. Temperature relationship and maximum heat transfer of hot and cold streams.

optimization efficiency.

Based on the above analysis, the inequality constraints of Eqs. (29) and (30) can be substituted by the feasible conversion formula of existence shown in Eq. (34), which can be used to update $Z_{i,j,k}$.

$$Z_{i,j,k} = Z_{i,j,k} \times \frac{\max(t_{i,k}^{in} - t_{j,k}^{out} - \Delta t_{\min},\ 0)}{t_{i,k}^{in} - t_{j,k}^{out} - \Delta t_{\min}} \quad i \in N_H, j \in N_C, k \in N_S \tag{34}$$

Although the prohibition of the matchings cannot guarantee that all solutions are feasible, it can remove a large number of infeasible solutions in the calculation, improve the quality of solutions, and provide a foundation for evolutionary computation.

5.2.2.2. Maximum energy matching strategy. In the superstructure model, there is a mutual restraint between heat transfer load and temperature constraints. The heat exchanger load generated randomly may violate the temperature constraints. Different from the model with the goal of minimizing matching (Bagajewicz and Valtinson, 2014; Papoulias and Grossmann, 1983; A Toffolo (2009b)), the maximum energy matching strategy developed in this study achieves the goal by maximizing the heat load and dynamically updating constraints, instead of directly optimizing the number of matches.

The maximum energy matching strategy which is a kind of greedy strategy, refers to setting the heat exchanger's load to the maximum value it can exchange. A heat exchanger's feasibility can be classified into two situations: the one shown in Fig. 9(a) is only constrained by the maximum heat transfer load of the streams, and the situation shown in Fig. 9(b) is constrained by both the temperature and the maximum heat transfer load. The key for the maximum energy matching to be feasible is to dynamically update the streams' inlet and outlet temperatures and the forbidden matching relationships. Since there is only one heat exchanger on each stream in each stage, the heat load computed through the maximum energy matching can fully meet the temperature constraints. After the maximum energy matching is performed for all stages, utility heat exchangers are added to streams whose heat exchange duty is not satisfied.

Based on the idea of dynamic programming, Eq. (22) and Eqs. (25)–(28) are dismissed, and the feasible conversion formulas of temperature and heat load are shown in Eqs. (35)–(37).

$$Q_{i,j,k} = Z_{i,j,k} \times \min\left(\left(t_{i,k}^{out} - T_j^{in}\right)\cdot F_j \cdot CP_j, \left(t_{j,k}^{in} - T_i^{out}\right)\cdot F_i \cdot CP_i\right) \quad i \in N_H, j \in N_C, k \in N_S \tag{35}$$

$$t_{i,k}^{in} = \begin{cases} T_i^{in} & k = 1, i \in N_H \\ T_i^{in} - \sum_{K=1}^{k}\sum_{j=1}^{N_C} Q_{i,j,K}/F_i \cdot CP_i & k \neq 1, i \in N_H, j \in N_C, k \in N_S \end{cases} \tag{36}$$

$$t_{j,k}^{out} = \begin{cases} T_j^{out} & k = 1, j \in N_C \\ T_j^{out} - \sum_{K=1}^{k}\sum_{i=1}^{N_H} Q_{i,j,K}/F_j \cdot CP_j & k \neq 1, i \in N_H, j \in N_C, k \in N_S \end{cases} \tag{37}$$

The HEN structure obtained by the maximum energy matching strategy is feasible with the minimum number of heat exchangers. Although only the energy target is considered, the maximum energy matching strategy can reduce the number of heat exchangers, thus saving the investment cost.

5.2.3. Strategies for improving operator

5.2.3.1. Decapitation and disaster strategy. The proposed model has a high degree of non-convexity and easily falls into the local optimum in the evolution. When the Pareto solution set does not change in three generations or more, the population cannot produce more diverse individuals through evolution. When the decapitation and disaster strategy is triggered, the Pareto front of the population will be eliminated, and the remaining individuals will be reduced by 50 % due to the catastrophe. The new individuals generated randomly are used to supplement the missing individuals. This strategy enables the population evolution to jump out of the local optimum.

5.2.3.2. Population migration strategy. A population's migration can bring a more abundant number of genes to the population. The population migration strategy requires each generation to have 10 % of individuals outflow and the same number for migration. Based on this strategy, the population genes' diversity can be ensured by randomly eliminating and generating 10 % of the population individuals.

5.2.3.3. Gene pool strategy. Whether or not the local optimal solution is the global optimal solution is unknown in the evolution process. A gene pool strategy is established to store the Pareto solution set of each generation during the evolution. When the decapitation and disaster strategy or population migration strategy is triggered, the local optimal solution will no longer participate in the evolution iteration. This strategy can ensure that the population evolution direction is to jump out of the local optimal solution while retaining the local optimal solution's gene and ensuring the global optimal solution is not eliminated. When the evolution reaches the number of iterations and jumps out of the cycle, the gene pool is merged with the final population to select the final Pareto solution set.

The NSGA-II improved based on the above strategies has better performance in multi-objective optimization of HEN, as it enhances the ability to jump out of local optima as well as the quality of initial solutions. The Pareto front and Utopian solution can be identified efficiently.

5.3. Optimization procedure

Based on the proposed model, strategies, and the improved NSGA-II algorithm, the HEN can be optimized in order to minimize the Excitation and energy consumption. The overall optimization procedure is shown in Fig. 10.

6. Case study

6.1. Case 1

This case is taken from Papoulias and Grossmann (1983) and is studied to test the performance of the proposed method. There are two hot and two cold streams. The stream data and cost parameters are taken from Papoulias and Grossmann (1983) and Zhang et al. (2011), as presented in Table 2.

When the minimum heat transfer temperature difference is set as 10 K, the optimization result without stream splitting reported in Papoulias and Grossmann (1983) is shown in Fig. 11. The equilibrium solution designed by the proposed method is demonstrated in Fig. 12 and

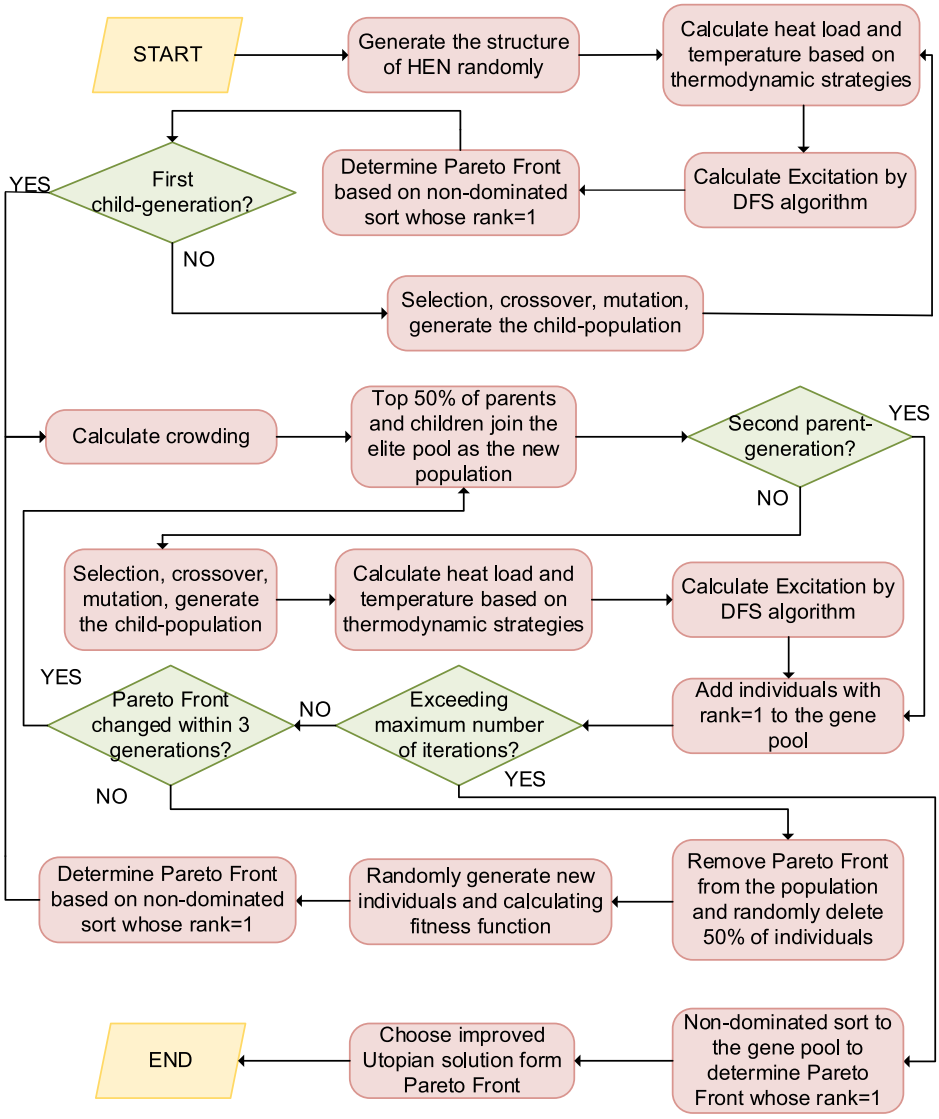

Fig.10. Overall procedure of the improved NSGA-II.

Table 2
Data of Case 1 (Papoulias and Grossmann, 1983).

Stream number	Temperature, K		Average heat capacity flow rate, kW·K^{-1}	Cost, $·kW·yr^{-1}
	inlet	outlet		
H1	443	333	30	
H2	423	303	15	
C1	293	408	20	
C2	353	413	40	
Steam	450	450		80
Cooling Water	293	313		20

Note: 1) Total heat transfer coefficient K = 0.8 (kW·m^2·K^{-1}) for all matches except ones involving steam
2) Total heat transfer coefficient K = 1.2 (kW·m^2·K^{-1}) for all matches involving steam

3) Annual investment cost equation from Papoulias and Grossmann (1983):
Annual cost = 1000 × [Area(m^2)]$^{0.6}$ ($·yr^{-1}) for all exchangers except heaters
Annual cost = 1200 × [Area(m^2)]$^{0.6}$ ($·yr^{-1}) for heaters
4) Annual investment cost equation from Zhang et al. (2011):
Annual cost = 15000 + 60 × [Area(m^2)]$^{0.8}$ ($·yr^{-1}) for all exchangers except heaters
Annual cost = 15000 + 30 × [Area(m^2)]$^{0.8}$ ($·yr^{-1}) for heaters

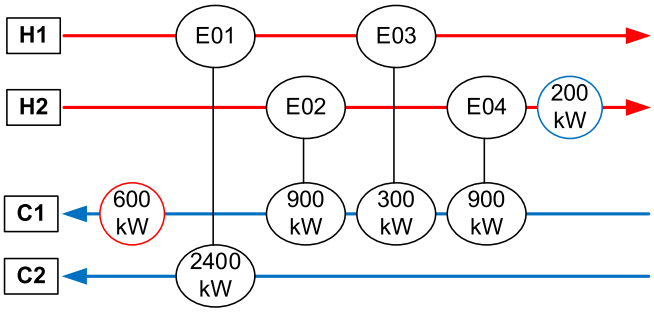

Fig.11. Result of Papoulias and Grossmann (1983) without stream splitting.

compared with that of Fig. 11 in Table 3. The utility consumption identified based on Papoulias and Grossmann's method (1983) is 42.86 % less than that of the equilibrium solution, while the heat exchanger area is 37.73 % greater, and the Excitation is 128.04 % higher.

Based on the cost equations reported by Papoulias and Grossmann (1983) and Zhang et al. (2011), the quality of optimization results in terms of the total annual cost will change, as shown in Table 3.

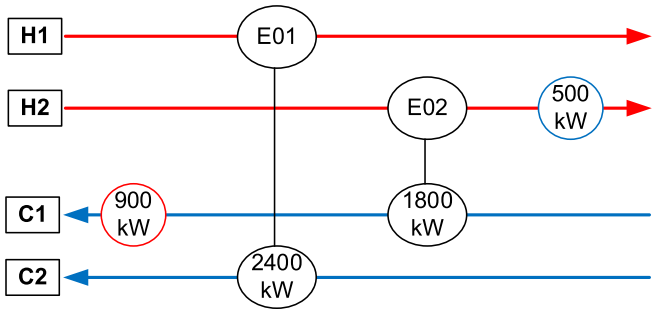

Fig.12. Equilibrium solution designed by proposed method.

This case shows that the proposed method can be used to identify the system with lower Excitation and even lower total annual cost. The annual investment cost equation and the trade-off between Excitation and total annual cost affect the optimization results.

6.2. Case 2

6.2.1. Coal-to-methanol process

A coal-to-methanol plant with an annual output of 551,880 tons of refined methanol is studied using the proposed method. The coal-water slurry gasification technology is adopted, and the generated crude syngas is deacidified and washed by low-temperature methanol. The clean syngas is converted into methanol in the methanol synthesis section; the

Table 3
Comparison of the results (Case 1).

	Utility consumption, kW	Heat exchange area, m^2	Excitation	Total annual cost, $\$\cdot yr^{-1}$ Based on Papoulias and Grossmann's cost equation	Based on Zhang et al's cost equation
Grossmann's work	800	354.1	4.31	89,832	126,646.62
This work	1,400	257.09	1.89	110,185.53	124,020.41

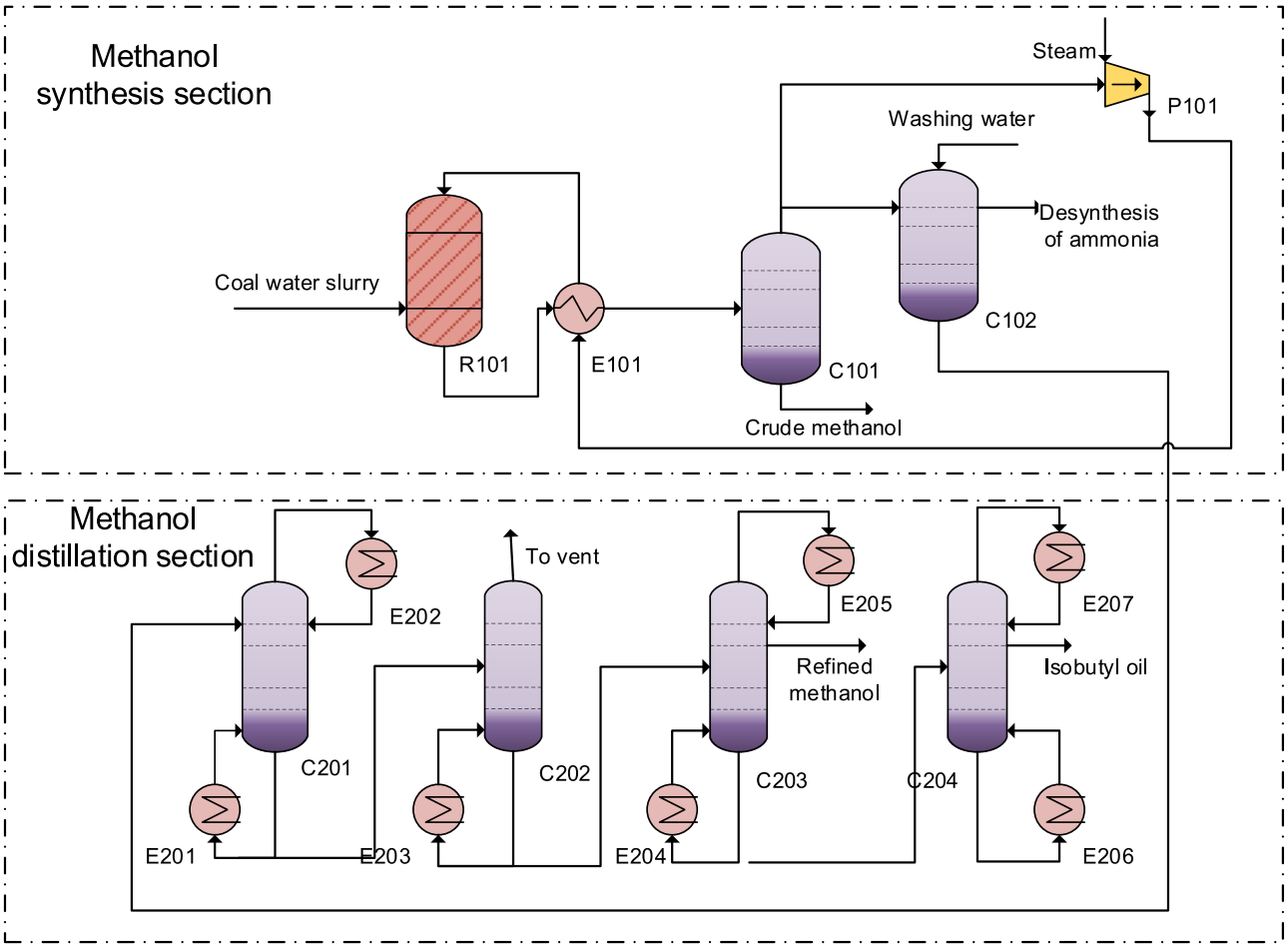

R101 - Coal to methanol reactor
P101 - Compressor
C101 - Methanol separator
C102 - Washing tower
C201 - Pre tower
C202 - Pressurized tower
C203 - Atmospheric tower
C204 - Recovery tower
Heat exchanger - E201 E202 E203 E204 E205 E206 E207

Fig.13. Flowchart of the methanol synthesis and distillation sections.

Table 4
Data of hot and cold streams.

Stream number	Temperature, ℃ inlet	outlet	Flow rate, kg·h^{-1}	Average heat capacity flow rate, kW·℃$^{-1}$	Heat load, kW
H1	242	30	279,623	284.67	39,854
H2	72	57	47,000	983.07	14,746
H3	57	54	2,480	28.33	85
H4	125	102	41,978	52.35	1,204
H5	112.6	44	34,800	33.01	2,278
H6	117	112.6	133,000	359,810	35,981
	0.4				
H7	68	53	119,517	2529	37,935
H8	51	31	32,500	27.65	553
H9	69	49	3,502	56.3	1,126
*H*10	109	40	8,114	9.75	673
C1	43	208	279,623	241.54	39,854
C2	40	61	70,715	63.81	1,340
C3	73	73.8	127,449	20,300	16,240
C4	74.3	89	76,778	81.9	1,204
C5	123	126	171,184	13,090	39,270
C6	109.2	109.3	67,191	359,810	35,981
C7	105	105.1		10,680	1,068

refined methanol is separated in the methanol distillation section, and by-product isobutyl oil is obtained; H_2S is sent to the desulfurization recovery section to generate sulfur. The methanol synthesis and distillation sections are the keys of this plant, and the corresponding flowchart is shown in Fig. 13. There are ten hot streams and seven cold streams, and their initial parameters are shown in Table 4. The minimum utility consumption of the system identified by the pinch analysis method is 109,206 kW. When all streams are heated or cooled by utilities, the Excitation is 0.

In the optimization, the parameters are set as follows:

1) The maximum population evolution is 15 generations;
2) The population size is 100 individuals;
3) The crossover rate is 50 %, the mutation probability is 5 %, and 30 children are generated per generation;
4) The minimum heat exchange temperature difference is 0.01 ℃.

Based on the proposed model, strategies, and the improved NSGA-II algorithm, HEN's optimization model is built and solved with Python 3.7. The solution is obtained in 101.97 s (The computer processor is Inter (R) Core (TM) i5-9300HCPU@2.40 GHz, and the RAM is 8.00G).

6.2.2. *Pareto front and improved Utopian solution*

The obtained minimum energy target and the minimum Excitation target evolution curves are shown in Fig. 14; the Pareto front is shown in Fig. 15.

The Utopian solution refers to the point with the smallest normalized Euclidean distance to the theory optimal point (109,206 kW, 0). Eq. (38) is used to calculate the normalized Euclidean distance.

However, the ideal solution is not the Utopian solution selected based on Eq. (38), for lower utility consumption remains our primary goal. Therefore, the quasi-gradient, shown in Eq. (39), will be introduced to facilitate the decision-making. The quasi-gradient, which is the normalized slope between two adjacent points and a non-positive number, reflects the variation degree of Excitation along with the energy targets. If the quasi-gradient is less than −10, a greater Excitation is acceptable and will not reduce the energy consumption significantly, and the improved Utopian solution, as shown in Fig. 16, is an equilibrium solution.

$$Distance_i = \sqrt{\left(\frac{Excitation_i - 0}{Excitation_{\max} - 0}\right)^2 + \left(\frac{Energy_i - 109,206}{Energy_{\max} - 109,206}\right)^2} \tag{38}$$

$$QG_i = \frac{Excitation_{i-1} - Excitation_i}{Energy_{i-1} - Energy_i} \times \frac{Energy_{\max} - 109,206}{Excitation_{\max} - 0} \tag{39}$$

6.2.3. *Comparison and analysis of selected solutions*

In order to highlight the superiority of the algorithm and the model, the improved Utopian solution is compared with three other solutions in Table 5. Besides, the HEN designed by the proposed method is compared with that designed by the Aspen Energy Analyzer. The specific data of the improved Utopian solution and comparison points 2 and 3 are illustrated in Appendix C. Comparison point 1 corresponds to the situation with all streams heated or cooled by the utilities and no heat exchange between streams. In this case, the Excitation of the HEN is 0, and the energy target is 271,903.77 kW.

The HEN of the improved Utopian solution is shown in Fig. 17, and the detailed data is shown in Table C1. There are four process stream heat exchangers and thirteen irrelevant subsystems. The maximum irrelevant subsystem includes three streams and two process stream heat

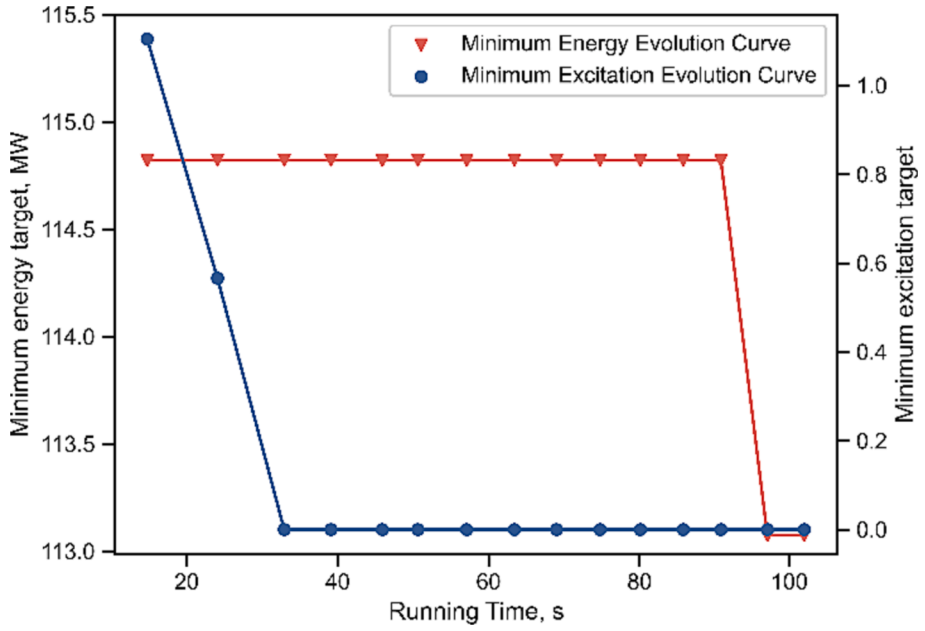

Fig.14. Optimization objectives' evolution curve.

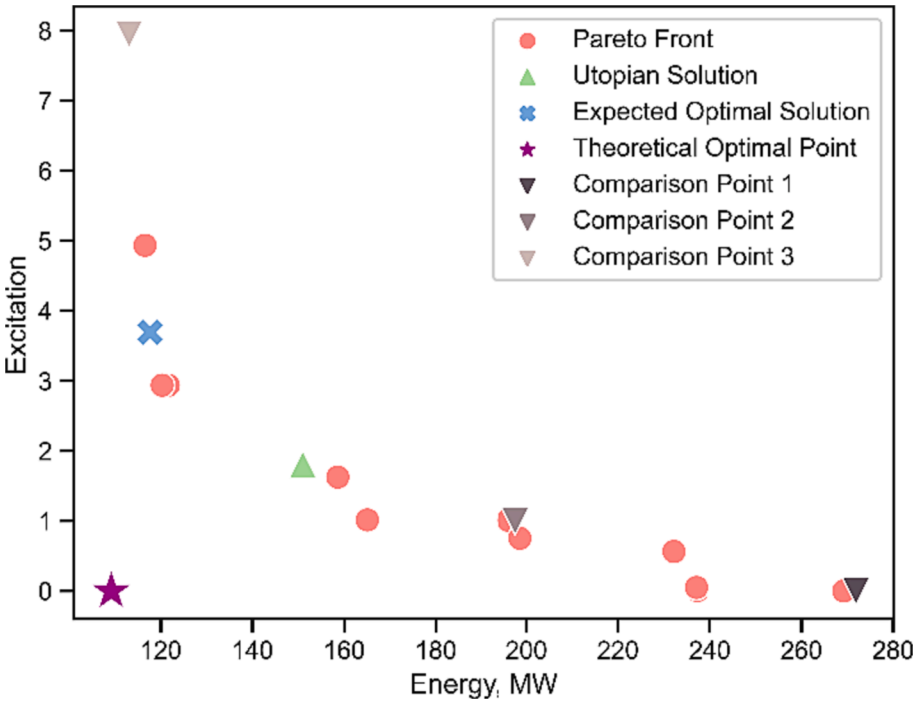

Fig.15. Pareto Front of the optimization.

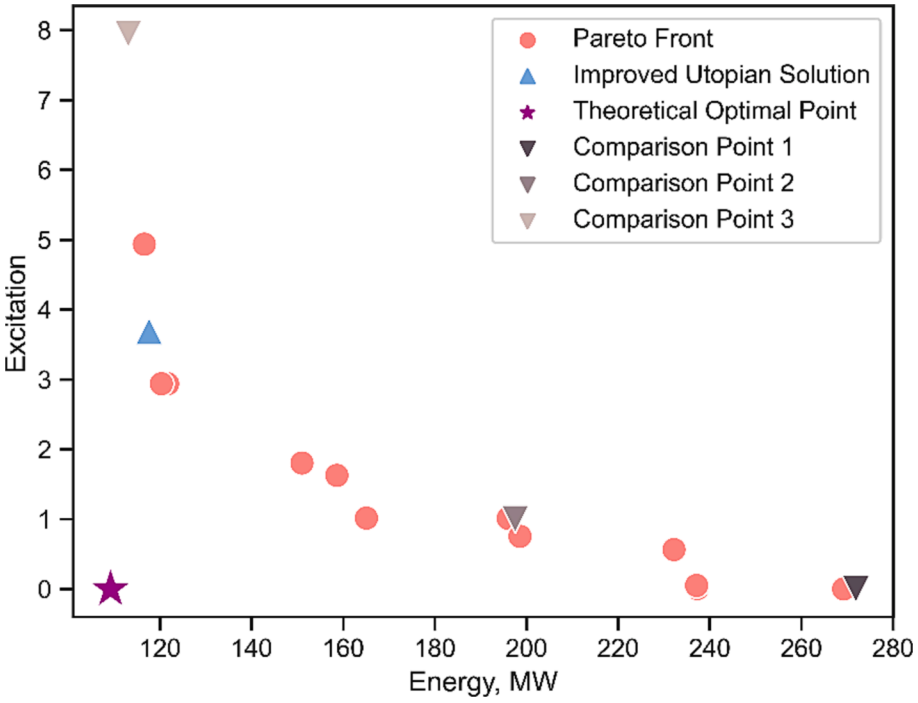

Fig.16. Pareto front and improved Utopian solution.

exchangers, and the secondary maximum irrelevant subsystem consists of two streams and one process stream heat exchanger. The heating utility consumption is 117,617 kW, and the Excitation is 3.69.

The HEN corresponding to comparison point 2 is shown in Fig. 18, and the detailed data is shown in Table C2. Comparison point 2 contains one process stream heat exchanger and 16 irrelevant subsystems; two irrelevant subsystems consist of two streams and one process stream heat exchanger. The heating utility consumption is 197,534 kW, and the Excitation is 1.

As analyzed in Section 3.3, the more the process stream heat exchangers, the fewer the irrelevant subsystems; the more heat exchangers in a single irrelevant subsystem, the more complex the network and the stronger the coupling. Correspondingly, the weaker the HEN's ability to resist parameter fluctuations, the greater the Excitation. Although the Excitation of comparison point 2 is less than that of the improved Utopian solution, the utility consumption is 67.9 % greater than that of the improved Utopian solution. Fig. 17 shows that the four heat exchangers of the improved Utopian solution have strong decoupling between each

Table 5
Comparison of the improved Utopian solution with three other solutions.

Point	Energy, kW	Excitation	Irrelevant subsystem	Process heat exchanger	Maximum irrelevant subsystem		Secondary maximum irrelevant subsystem	
					No. of streams	No. of heat exchangers	No. of streams	No. of heat exchangers
Improved Utopian solution	117,617	3.69	13	4	3	2	2	1
Comparison point 1	271,904	0.00	17	0	1	0	1	0
Comparison point 2	197,534	1.00	15	2	2	1	2	1
Comparison point 3	113,073	7.95	10	7	3	2	3	2
Aspen result	152,490	13.45	10	7	8	7	1	0

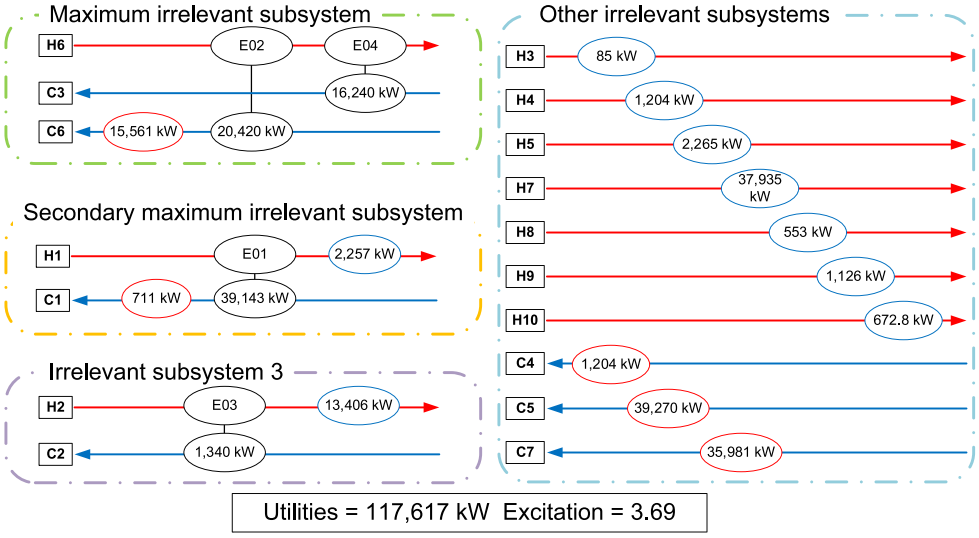

Fig.17. HEN corresponding to the improved Utopian solution.

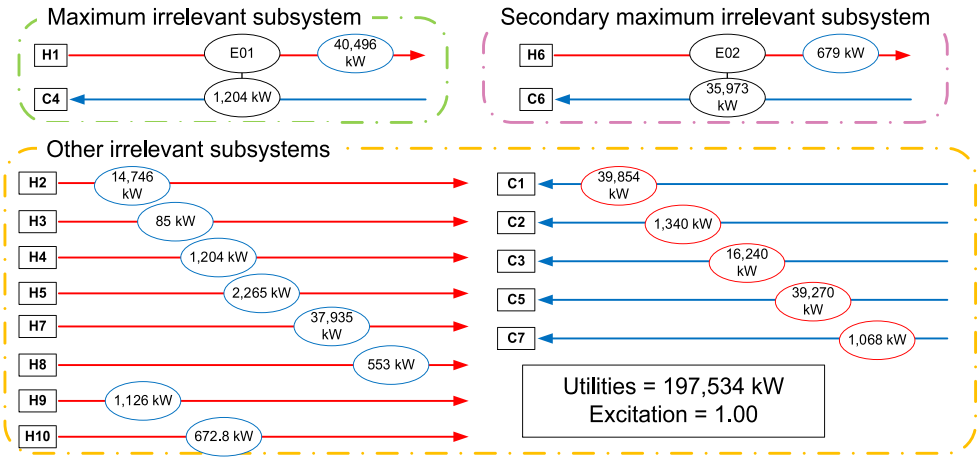

Fig.18. HEN corresponding to the comparison point 2.

other, and the Excitation is within an acceptable range. Therefore, the improved Utopian solution is better than comparison point 2.

The HEN corresponding to comparison point 3 is shown in Fig. 19, and the detailed data is shown in Table C3. There are seven process stream heat exchangers and ten irrelevant subsystems. Two subsystems include three streams and two process stream heat exchangers. Compared with the improved Utopian solution, comparison point 3 has more process stream heat exchangers and fewer irrelevant subsystems, significantly enhancing the coupling between heat exchangers. Its heating utility consumption is 113,073 kW, 2.3 % less than the improved Utopian solution, while the Excitation is 7.95, 116.6 % greater than that of the improved Utopian solution. Therefore, the improved Utopian solution is better than comparison point 3.

The HEN designed by Aspen Energy Analyzer is shown in Fig. 20, which includes seven process stream heat exchangers and ten irrelevant subsystems. The maximum irrelevant subsystem contains eight streams and seven process stream heat exchangers. The coupling between these heat exchangers is much stronger, as the Excitation (13.45) is 264.50 % greater, and its energy target is 30.8 % greater than the improved Utopian solution. Therefore, the HEN designed by the Aspen Energy Analyzer is inferior to the improved Utopian solution.

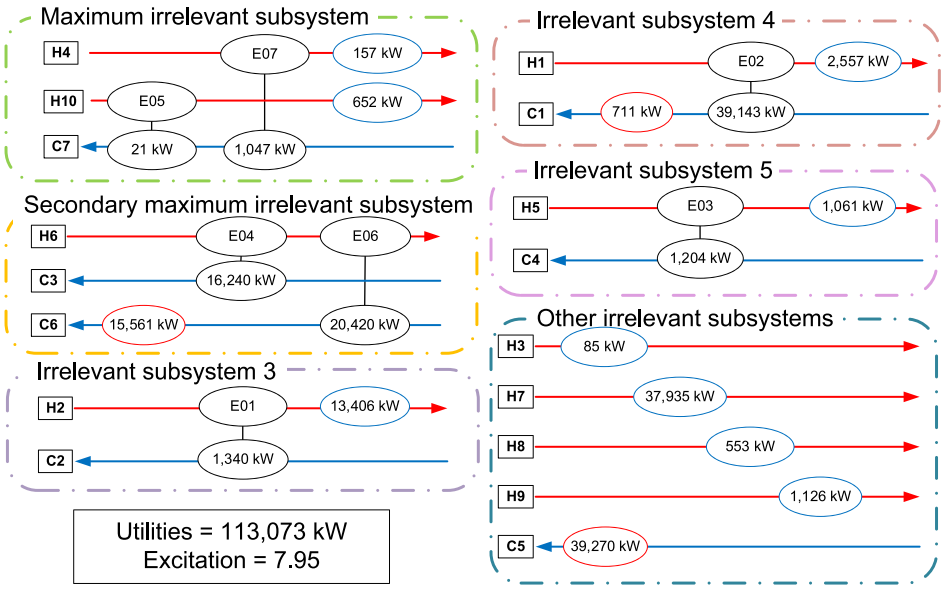

Fig.19. HEN corresponding to the comparison point 3.

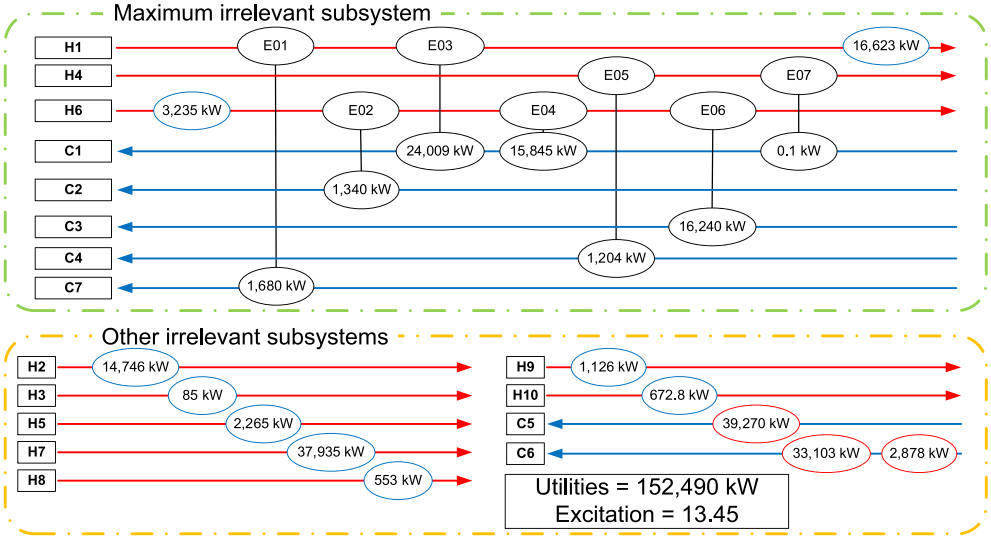

Fig.20. The HEN Designed by Aspen Energy Analyzer.

Table 6
Total heat transfer coefficient.

Process stream heat exchanger	Cooler	Heater
0.5 kW·°C $^{-1}$·m^{-2}	0.714 kW·°C $^{-1}$·m^{-2}	0.667 kW·°C $^{-1}$·m^{-2}

Table 7
Utility parameters.

Utility	Cost, \$·kg^{-1}	Heat capacity, kJ·°C $^{-1}$·kg^{-1}	Difference between inlet and outlet temperatures, ℃
20℃ cooling water	2.38 × 10^{-5}	4.183	10
2 MPa steam	1.31 × 10^{-2}	2,796.4	1

6.2.4. *Economic analysis*

In order to verify the superiority of the improved Utopian solution further, the economic performance of the improved Utopian solution and comparison point 3 are compared.

The total cost of the HEN, the annualized investment cost, and the annual operating cost are calculated in Eqs. (40)–(42), respectively.

$$COST_{total} = \sum_{i=1}^{n} COST_{investment,i} + \sum_{j=1}^{m} COST_{utility,j} \tag{40}$$

$$COST_{investment,i} = \frac{COST_{fixed} + \alpha area_i^{\beta}}{Year} \tag{41}$$

$$COST_{utility,j} = Hour \times \gamma QU_j \tag{42}$$

Where $COST$ denotes the annualized cost, \$·y^{-1}; n is the number of heat exchangers; m is the number of utility heat exchangers; $COST_{fixed}$ stands for the fixed investment cost of the heat exchanger and is taken as 90,400 \$ (Sreepathi and Rangaiah, 2014); *area* is the heat transfer area,

m^2; α and β are constants and taken as 1,127 and 0.998; *Year* is the depreciation years of heat exchanger, y; *Hour* is the annual operating time of the heat exchanger, $h{\cdot}y^{-1}$; *QU* is the heat load of the utility heat exchanger, kW; γ is the utility cost coefficient, $\${\cdot}kJ^{-1}$, and can be calculated according to Eq. (43).

$$\gamma = \frac{CM}{CpM \times \Delta T} \tag{43}$$

Where *CM* is the media costs of utilities, $\${\cdot}kg^{-1}$; ΔT is the temperature difference between the inlet and outlet medium, °C; *CpM* is the heat capacity or latent heat of the medium, $kJ{\cdot}{}^{\circ}C^{-1}{\cdot}kg^{-1}$。

According to Sreepathi and Rangaiah (2014), the total heat transfer coefficient of the heat exchanger is set and shown in Table 6. The depreciation period is ten years, and the annual operating time is 8,000 $h{\cdot}y^{-1}$. The parameters related to the utilities are shown in Table 7. The detailed data for the improved Utopian solution and comparison point 3 are shown in Table D1 and D2 in Appendix D.

Based on the economic analysis, the annualized cost of the improved Utopian solution is 12.1576 million $\${\cdot}y^{-1}$, while that of comparison point 3 is 12.2518 million $\${\cdot}y^{-1}$. Although comparison point 3 requires less energy, its economic performance is inferior to the improved Utopian solution. Selecting a Utopian solution based on Eq. (39) is effective and reasonable. With the energy and Excitation targets taken into account, the proposed method can obtain a solution with a lower total cost.

7. Conclusions

A novel method is proposed to design HEN with high resistance to parameter fluctuations and evaluate the practical HEN from a decoupling perspective. Based on the Digraph, Adjacency matrix, Incidence matrix, Reachability matrix, and Laplacian matrix, which are firstly used for HEN synthesis, the HEN's topology structure can be comprehensively illustrated; the HEN's fluctuation transmission mechanism and path can be identified efficiently. The relationship between the HEN and the degree of disturbance can be identified by transforming the Excitation into a graph theory problem. The multi-objective optimization mathematical model with Excitation and energy consumption as the objectives can be used to optimize the HEN and target the one with strong resistance to fluctuations. Combined NSGA-II and DFS algorithms solve this model efficiently; the proposed strategies can enhance the solving efficiency and improve the solutions' quality.

The study of two cases demonstrates that the proposed method performs better than the literature methods. The study of a coal-to-methanol process shows that the proposed method and algorithm can effectively design HENs with strong resistance to uncertain parameters under the premise of an insignificant increase in utility consumption. For a practical HEN, it can be used to evaluate the overall impact of parameter fluctuations. In addition, the proposed correlation between graph theory and HEN is also instructive for analyzing the parameter fluctuations between different units and provides technical support for the digital twin of the chemical process. Besides, machine learning driven combinatorial optimization is tightly related to graphs (Bengio et al., 2021; Dai et al., 2017), and transforming HEN into graph problems also lay a solid theoretical foundation for machine learning driven HEN optimization.

In the proposed method, only the isothermal mixing is considered, and stream splitting is ignored. The non-isothermal mixing and the stream splitting cannot be directly applied, and the corresponding improvement should be considered in the future. Besides, the model can be extended with the reaction and separation units considered. Although the topological structure between different units and the HEN is generally straightforward, sensitivity analysis is often tricky due to the complexity of reaction and separation systems. The hybrid modeling method will be employed to simplify the problem so as to realize the optimization of the whole system.

CRediT authorship contribution statement

Zixuan Zhang: Data curation, Formal analysis, Methodology, Software, Conceptualization, Writing – original draft. **Liwen Zhao:** Conceptualization, Investigation, Resources, Software, Validation. **Ibrahim Tera:** Validation, Visualization, Resources. **Guilian Liu:** Conceptualization, Funding acquisition, Project administration, Supervision, Writing – review & editing.

Declaration of competing interest

The authors declare that they have no known competing financial interests or personal relationships that could have appeared to influence the work reported in this paper.

Data availability

Data will be made available on request.

Acknowledgements

Financial support provided by the National Natural Science Foundation of China (22078259) and the Department of Science and Technology of Inner Mongolia (CN) (2023YFHH0108) are gratefully acknowledged.

Appendix A

Table A1
Pseudo-code of targeting the reachable matrix by the multiplication algorithm.

Input:*Adjacency Matrix*(*Adj*)	
Output:*Accessibility Matrix*(*Acc*)	
1	***S*** = ***Adj*** + ***I*** //***S*** is self-multiplication matrix , ***I*** is identity matrix.
2	***While (M*** is different before and after iteration.***):***
3	***If(*** first iteration***):***
4	M = S⊙S //⊙ represents Boolean operation.
5	***Else:***
6	M = M⊙S
7	Acc = M - I

Appendix B

When there are disturbances in a stream's flowrate or heat capacity, which is caused by the composition variation, the partial derivative over

decision variables can be discussed by a similar method to the disturbance in temperature. In this case, Eq. (5) is a linear equation, and hence *F* and *CP* can be considered as one variable. Eq. (6) is independent from *FCP*. When *FCP* changes, $\frac{\partial Eq}{\partial S}$ is the same as that when temperature changes, since the state variable is still the outlet temperature of the heat exchanger. The partial derivatives over decision variables are shown in Table B1.

Table B1
The partial derivative over decision variables when *FCP* changes.

	Decision variable	Partial derivative of balance equation	Partial derivative of heat-transfer equation
$\frac{\partial Eq}{\partial \boldsymbol{D}}$	Cold stream's inlet *FCP*	$\frac{\partial Eq}{\partial \boldsymbol{D}} = t_C^{out} - t_C^{in}$	$\frac{\partial Eq}{\partial \boldsymbol{D}} = 0$
	Hot stream's inlet *FCP*	$\frac{\partial Eq}{\partial \boldsymbol{D}} = -\left(t_H^{in} - t_H^{out}\right)$	$\frac{\partial Eq}{\partial \boldsymbol{D}} = 0$
	The inlet *FCP* of cold and hot streams	$\frac{\partial Eq}{\partial \boldsymbol{D}} = \left(t_C^{out} - t_C^{in}\right) - \left(t_H^{in} - t_H^{out}\right)$	$\frac{\partial Eq}{\partial \boldsymbol{D}} = 0$

Appendix C

Table C1
Details of the Utopian Solution.

Heat exchangers	Streams	Inlet temperature, °C	Outlet temperature, °C	Heat capacity flow rate, kW■°C $^{-1}$	Heat flux, kW	Utility consumption, kW
E01	H1	242.00	43.00	196.70	39,143.30	
	C1	43.00	205.06	241.54		
E02	H6	117.40	114.73	7,637.50	20,420.00	
	C6	109.20	109.26	359,810.00		
E03	H2	72.00	70.64	983.07	1,340.01	
	C2	40.00	61.00	63.81		
E04	H6	114.73	112.60	7,637.50	16,240.00	
	C3	73.00	73.80	20,300.00		
EH1	C1	205.06	208.00	241.54	710.80	117,617.15
EH2	C4	74.30	89.00	81.90	1,203.93	
EH3	C5	123.00	126.00	13,090.00	39,270.00	
EH4	C6	109.26	109.30	359,810.00	15,561.00	
EH5	C7	105.00	105.10	10,680.00	1,068.00	
EC1	H1	43.00	30.00	196.70	2,557.10	
EC2	H2	70.64	57.00	983.07	13,406.04	
EC3	H3	57.00	54.00	28.33	84.99	
EC4	H4	125.00	102.00	52.35	1,204.05	
EC5	H5	112.60	44.00	33.01	2,264.49	
EC6	H7	68.00	53.00	2,529.00	37,935.00	
EC7	H8	51.00	31.00	27.65	553.00	
EC8	H9	69.00	49.00	56.30	1,126.00	
EC9	*H*10	109.00	40.00	9.75	672.75	

Table C2
Details of the comparison point 2.

Heat exchangers	Streams	Inlet temperature, °C	Outlet temperature, °C	Heat capacity flow rate, kW■°C $^{-1}$	Heat flux, kW	Utility consumption, kW
E01	H1	242.00	236.57	196.70	1,068.00	
	C7	105.00	105.10	10,680.00		
EC1	H1	236.57	30.00	196.70	40,632.32	269,767.77
EC2	H2	72.00	57.00	983.07	14,746.05	
EC3	H3	57.00	54.00	28.33	84.99	
EC4	H4	125.00	102.00	52.35	1,204.05	
EC5	H5	112.60	44.00	33.01	2,264.49	
EC6	H6	117.40	112.60	7,637.50	36,660.00	
EC7	H7	68.00	53.00	2,529.00	37,935.00	
EC8	H8	51.00	31.00	27.65	553.00	
EC9	H9	69.00	49.00	56.30	1,126.00	
EC10	*H*10	109.00	40.00	9.75	672.75	
EH1	C1	43.00	208.00	241.54	39,854.10	
EH2	C2	40.00	61.00	63.81	1,340.01	
EH3	C3	73.00	73.80	20,300.00	16,240.00	
EH4	C4	74.30	89.00	81.90	1,203.93	
EH5	C5	123.00	126.00	13,090.00	39,270.00	
EH6	C6	109.20	109.30	359,810.00	35,981.00	

Table C3
Details of the comparison point 3.

Heat exchangers	Streams	Inlet temperature, °C	Outlet temperature, °C	Heat-capacity flow rate, kW■°C $^{-1}$	Heat flux, kW	Utility consumption, kW
E01	H1	242.00	43.00	196.70	39,143.30	
	C1	43.00	205.06	10,680.00		
E02	H6	117.40	115.60	7,637.50	13,758.75	
	C3	73.12	73.80	20,300.00		
E03	H4	125.00	102.00	52.35	1,204.05	
	C3	73.06	73.12	20,300.00		
E04	H5	112.60	73.00	33.01	1,307.20	
	C3	73.00	73.06	20,300.00		
E05	H6	117.40	115.60	7,637.50	21,727.32	
	C6	109.20	109.26	35,9810.00		
E06	H2	72.00	70.64	983.07	1,340.01	
	C2	40.00	61.00	63.81		
E07	H6	115.60	112.76	7,637.50	1,203.93	
	C4	74.30	89.00	81.90		
EC1	H1	43.00	30.00	196.70	2,257.10	112,594.65
EC2	H2	70.64	57.00	983.07	13,406.04	
EC3	H3	57.00	54.00	28.33	84.99	
EC4	H5	73.00	44.00	33.01	957.29	
EC5	H7	68.00	53.00	2529.00	37,935.00	
EC6	H8	51.00	31.00	27.65	553.00	
EC7	H9	69.00	49.00	56.30	1,126.00	
EC8	*H*10	109.00	40.00	9.75	672.75	
EH1	C1	208.00	205.06	241.54	710.80	
EH2	C5	123.00	126.00	13,090.00	39,270.0	
EH3	C6	109.26	109.30	359,810.00	14,253.68	
EH4	C7	105.00	105.10	10,680.00	1,068.00	

Appendix D

Table D1
Details of Utopian Solution Cost.

Heat exchangers	Heat flux, kW	Heat area, m^{-2}	Investment cost, 10^3 $	Utility cost, 10^3 $
E01	39,143.30	17,408.26	19,330.08	
E02	20,420.00	6,040.89	6,780.96	
E03	1,340.01	139.72	246.31	
E04	16,240.00	806.57	987.31	
EH1	710.80	370.96	503.55	932.77
EH2	1,203.93	14.13	106.24	
EH3	39,270.00	692.60	860.82	
EH4	15,561.00	232.76	349.88	
EH5	1,068.00	15.33	107.58	
EC1	2,557.10	311.68	437.66	7,938.16
EC2	13,406.04	483.31	628.40	
EC3	84.99	3.91	94.80	
EC4	1,204.05	19.08	111.77	
EC5	2,264.49	66.83	165.08	
EC6	37,935.00	1,496.67	1,752.66	
EC7	553.00	49.92	146.22	
EC8	1,126.00	46.65	142.57	
EC9	672.75	21.92	114.95	
Sum of individual annualized, million $·y^{-1}			3.2867	8.8709
Total annualized, million $·y^{-1}			12.1576	

Table D2
Details of Comparison Point 3 Cost.

Heat exchangers	Heat flux, kW	Heat area, m^{-2}	Investment cost, 10^3 $	Utility cost, $10^3$$
E01	1,340.01	139.72	246.31	
E02	39,143.30	17,408.26	19,330.08	
E03	1,203.93	282.33	405.02	
E04	16,240.00	756.34	931.57	
E05	21.00	15.60	107.89	
E06	20,420.00	8,888.08	9,926.76	
E07	1,047.00	799.27	979.22	
EH1	710.80	370.96	503.55	896.11
EH2	39,270.00	692.60	860.82	
EH3	15,561.00	232.76	349.88	
EC1	2,557.10	311.68	437.66	7,636.59
EC2	13,406.04	483.31	628.40	
EC3	84.99	3.91	94.80	

(*continued on next page*)

Table D2 (*continued*)

Heat exchangers	Heat flux, kW	Heat area, m^{-2}	Investment cost, 10^3 $	Utility cost, $10^3$$
EC4	157.05	2.80	93.55	
EC5	1,060.56	43.79	139.38	
EC6	37,935.00	1,496.67	1,752.66	
EC7	553.00	49.92	146.22	
EC8	1,126.00	46.65	142.57	
EC9	651.75	21.59	114.58	
Sum of individual annualized, million $\$\cdot y^{-1}$			3.7191	8.5327
Total annualized, million $\$\cdot y^{-1}$			12.2518	

References

Aguilera, N., Nasini, G., 1995. Flexibility test for heat exchanger networks with uncertain flowrates. Comput. Chem. Eng. 19, 1007–1017. https://doi.org/10.1016/0098-1354(95)99934-B.

Akutsu, T., Tamura, T., 2012. A Polynomial-Time Algorithm for Computing the Maximum Common Subgraph of Outerplanar Graphs of Bounded Degree, in: Rovan, B., Sassone, V., Widmayer, P. (Eds.), Kyoto University. Presented at the Mathematical Foundations of Computer Science 2012, pp. 76–87.

Bagajewicz, M., Valtinson, G., 2014. On the minimum number of units in heat exchanger networks. Ind. Eng. Chem. Res. 53, 16899–16904. https://doi.org/10.1021/ie402324j.

Bengio, Y., Lodi, A., Prouvost, A., 2021. Machine learning for combinatorial optimization: a methodological tour d'horizon. Eur. J. Oper. Res. 290, 405–421. https://doi.org/10.1016/j.ejor.2020.07.063.

Calandranis, J., Stephanopoulos, G., 1986. Structural operability analysis of heat-exchanger networks. Chem. Eng. Res. Des. 64, 347–364.

Cardoso-Fernández, V., Bassam, A., May Tzuc, O., Barrera Ch., M.A., Chan-González, J. de J., Escalante Soberanis, M.A., Velázquez-Limón, N., Ricalde, L.J., 2023. Global sensitivity analysis of a generator-absorber heat exchange (GAX) system's thermal performance with a hybrid energy source: An approach using artificial intelligence models. Applied Thermal Engineering 218, 119363. https://doi.org/10.1016/j.applthermaleng.2022.119363.

Cerda, J., Galli, M., 1990. Synthesis of flexible heat-exchanger networks.2. nonconvex networks with large temperature-variations. Comput. Chem. Eng. 14, 213–225. https://doi.org/10.1016/0098-1354(90)87079-5.

Cerda, J., Galli, M., Camussi, N., Isla, M., 1990. Synthesis of flexible heat-exchanger networks.1. convex networks. Comput. Chem. Eng. 14, 197–211. https://doi.org/10.1016/0098-1354(90)87078-4.

Charnkhuang, Y., Lee, J.-Y., Foo, D.C.Y., 2020. Retrofit of Heat Exchanger Networks with Temperature and Flowrate Uncertainties, in: Pierucci, S., Manenti, F., Bozzano, G.L., Manca, D. (Eds.), Computer Aided Chemical Engineering, 30 European Symposium on Computer Aided Process Engineering. Elsevier, pp. 1525–1530. https://doi.org/10.1016/B978-0-12-823377-1.50255-X.

Chen, S., Liang, L., Tian, Y., 2015. The number of connected components in a graph associated with a rectangular (0,1)-matrix. Linear Algebra Appl. 487, 74–85. https://doi.org/10.1016/j.laa.2015.09.018.

Chew, Y.E., Gan, Z.W., Heng, H., Nair, P.N.S.B., Tan, R.R., Foo, D.C.Y., 2023. Carbon emissions pinch analysis (CEPA) for emissions reduction and energy planning in Canada. Clean Techn. Environ. Policy 25, 2413–2431. https://doi.org/10.1007/s10098-023-02537-9.

Coello Coello, C.A., Christiansen, A.D., 1995. Approach to multiobjective optimization using genetic algorithms. Presented at the Intelligent Engineering Systems through Artificial Neural Networks 411–416.

Dai, H., Khalil, E.B., Zhang, Y., Dilkina, B., Song, L., 2017. Learning combinatorial optimization algorithms over graphs. Presented at the Advances in Neural Information Processing Systems 6349–6359.

Deb, K., Pratap, A., Agarwal, S., Meyarivan, T., 2002. A fast and elitist multiobjective genetic algorithm: NSGA-II. IEEE Trans. Evol. Comput. 6, 182–197. https://doi.org/10.1109/4235.996017.

Deo, N., 1975. Graph theory with applications to engineering and computer science. Networks 5, 299–300. https://doi.org/10.1002/net.1975.5.3.299.

Floudas, C.A., Ciric, A.R., Grossmann, I.E., 1986. Automatic synthesis of optimum heat exchanger network configurations. AIChE J. 32, 276–290. https://doi.org/10.1002/aic.690320215.

Fonseca, C.M., Fleming, P.J., 1995. Multiobjective genetic algorithms made easy: Selection, sharing and mating restriction. Presented at the IEE Conference Publication, pp. 45–52. https://doi.org/10.1049/cp:19951023.

Francesconi, J.A., Oliva, D.G., Aguirre, P.A., 2017. Flexible heat exchanger network design of an ethanol processor for hydrogen production. A model-based multi-objective optimization approach. Int. J. Hydrogen Energy 42, 2736–2747. https://doi.org/10.1016/j.ijhydene.2016.10.156.

Galli, M., Cerda, J., 1991. Synthesis of flexible heat-exchanger networks.3. temperature and flow-rate variations. Comput. Chem. Eng. 15, 7–24. https://doi.org/10.1016/0098-1354(91)87002-Q.

Galli, M., Cerda, J., 1998. A customized MILP approach to the synthesis of heat recovery networks reaching specified topology targets. Ind. Eng. Chem. Res. 37, 2479–2495. https://doi.org/10.1021/ie9705564.

Galli, M., Cerdá, J., 2001. Retrofit of heat exchanger networks with topology changes under designer control. Lat. Am. Appl. Res. 31, 247–254.

Gambardella, L.M., Dorigo, M., 1996. Solving symmetric and asymmetric TSPs by ant colonies. Presented at the Proceedings of the IEEE Conference on Evolutionary Computation, pp. 622–627.

Grossmann, I., Halemane, K., Swaney, R., 1983. Optimization strategies for flexible chemical processes. Comput. Chem. Eng. 7, 439–462. https://doi.org/10.1016/0098-1354(83)80022-2.

Gu, K., Vassiliadis, V.S., 2014. Limitations in using Euler's formula in the design of heat exchanger networks with Pinch Technology. Comput. Chem. Eng. 68, 123–127. https://doi.org/10.1016/j.compchemeng.2014.05.015.

Gura, K., Hirst, J., Mummert, C., 2015. On the existence of a connected component of a graph. Computability-the Journal of the Association CIE 4, 103–117. https://doi.org/10.3233/COM-150039.

Hafizan, A.M., Klemeš, J.J., Alwi, S.R.W., Manan, Z.A., Hamid, M.K.A., 2019. Temperature disturbance management in a heat exchanger network for maximum energy recovery considering economic analysis. Energies 12, 594. https://doi.org/10.3390/en12040594.

Haimes, Lasdon, L., Wismer, D., 1971. On a bicriterion formation of the problems of integrated system identification and system optimization. IEEE Transactions on Systems, Man and Cybernetics SMC-1, 296–297. https://doi.org/10.1109/TSMC.1971.4308298.

Jiang, N., Shelley, J.D., Doyle, S., Smith, R., 2014. Heat exchanger network retrofit with a fixed network structure. Appl. Energy 127, 25–33. https://doi.org/10.1016/j.apenergy.2014.04.028.

Kang, L., Liu, Y., 2018a. A three-step method to improve the flexibility of multiperiod heat exchanger networks. Process Integration and Optimization for Sustainability 2, 169–181. https://doi.org/10.1007/s41660-018-0034-5.

Kang, L., Liu, Y., 2018b. Design of flexible multiperiod heat exchanger networks with debottlenecking in subperiods. Chem. Eng. Sci. 185, 116–126. https://doi.org/10.1016/j.ces.2018.04.017.

Kang, L., Tang, W., Liu, Y., Daoutidis, P., 2016. Control configuration synthesis using agglomerative hierarchical clustering: A graph-theoretic approach. J. Process Control 46, 43–54. https://doi.org/10.1016/j.jprocont.2016.07.009.

Kann, V., 1992. On the approximability of the maximum common subgraph problem. Lect. Notes Comput. Sci 577, 377–388. https://doi.org/10.1007/3-540-55210-3_198.

Kemp, I.C., 2007. Key concepts of pinch analysis. In: Kemp, I.C. (Ed.), Pinch Analysis and Process Integration (second Edition). Butterworth-Heinemann, Oxford, pp. 15–40. https://doi.org/10.1016/B978-075068260-2.50007-9.

Kisala, T., Trevinolozano, R., Boston, J., Britt, H., 1987. Sequential modular and simultaneous modular strategies for process flowsheet optimization. Comput. Chem. Eng. 11, 567–579. https://doi.org/10.1016/0098-1354(87)87003-5.

Lee, J.-Y., Bai, P.-F., Ooi, R.E.H., Foo, D.C.Y., Tan, R.R., 2021. Planning of non-conventional gas field development with parametric uncertainties, in: Türkay, M., Gani, R. (Eds.), Computer Aided Chemical Engineering, 31 European Symposium on Computer Aided Process Engineering. Elsevier, pp. 1865–1870. https://doi.org/10.1016/B978-0-323-88506-5.50289-8.

Lee, J.-Y., Tsai, C.-H., Foo, D.C.Y., 2020. Single and multi-objective optimisation for the retrofit of process water networks. J. Taiwan Inst. Chem. Eng. 117, 39–47. https://doi.org/10.1016/j.jtice.2020.11.026.

Letsios, D., Kouyialis, G., Misener, R., 2018. Heuristics with performance guarantees for the minimum number of matches problem in heat recovery network design. Comput. Chem. Eng. 113, 57–85. https://doi.org/10.1016/j.compchemeng.2018.03.002.

Li, J., Du, J., Zhao, Z., Yao, P., 2014a. Structure and area optimization of flexible heat exchanger networks. Ind. Eng. Chem. Res. 53, 11779–11793. https://doi.org/10.1021/ie501278c.

Li, J., Du, J., Zhao, Z., Yao, P., 2014b. Synthesis of large-scale multi-stream heat exchanger networks using a stepwise optimization method. J. Taiwan Inst. Chem. Eng. 45, 508–517. https://doi.org/10.1016/j.jtice.2013.06.033.

Li, J., Du, J., Zhao, Z., Yao, P., 2015. Efficient method for flexibility analysis of large-scale nonconvex heat exchanger networks. Ind. Eng. Chem. Res. 54, 10757–10767. https://doi.org/10.1021/acs.iecr.5b00237.

Linnhoff, B., Hindmarsh, E., 1983. The pinch design method for heat exchanger networks. Chem. Eng. Sci. 38, 745–763. https://doi.org/10.1016/0009-2509(83)80185-7.

Linnhoff, B., Kotjabasakis, E., 1986. Downstream paths for operable process design. Chem. Eng. Prog. 82, 23–28.

Lv, J., Jiang, X., He, G., Xiao, W., Li, S., Sengupta, D., El-Halwagi, M.M., 2017. Economic and system reliability optimization of heat exchanger networks using NSGA-II algorithm. Applied Thermal Engineering 124, 716–724. https://doi.org/10.1016/j.applthermaleng.2017.05.154.

Miranda, C.B., Costa, C.B.B., Caballero, J.A., Ravagnani, M.A.S.S., 2016. Heat exchanger network optimization for multiple period operations. Ind. Eng. Chem. Res. 55, 10301–10315. https://doi.org/10.1021/acs.iecr.6b01117.

Mohanan, K., Jogwar, S.S., 2022. Optimal operation of heat exchanger networks through energy flow redistribution. AIChE J 68, e17716.

Moore, J., Chapman, R., Dozier, G., 2000. Multiobjective particle swarm optimization. In: Presented at the Proceedings of the Annual Southeast Conference, pp. 56–57. https://doi.org/10.1145/1127716.1127729.

Morari, M., 1983. Flexibility and resiliency of process systems. Comput. Chem. Eng. 7, 423–437. https://doi.org/10.1016/0098-1354(83)80021-0.

Nair, P.N.S.B., Tan, R.R., Foo, D.C.Y., Gamaralalage, D., Short, M., 2023. DECO2—an open-source energy system decarbonisation planning software including negative emissions technologies. Energies 16, 1708. https://doi.org/10.3390/en16041708.

Papoulias, S.A., Grossmann, I.E., 1983. A structural optimization approach in process synthesis—II: Heat recovery networks. Comput. Chem. Eng. 7, 707–721. https://doi.org/10.1016/0098-1354(83)85023-6.

Pareto, V., 1955. L'économie pure. Metroeconomica 7, 1–15. https://doi.org/10.1111/j.1467-999X.1955.tb00736.x.

Pavão, L.V., Costa, C.B.B., Ravagnani, M.A.S.S., Jiménez, L., 2017. Costs and environmental impacts multi-objective heat exchanger networks synthesis using a meta-heuristic approach. Appl. Energy 203, 304–320. https://doi.org/10.1016/j.apenergy.2017.06.015.

Payet, L., Hétreux, R., Hétreux, G., Bourgeois, F., Floquet, P., 2018. Flexibility assessment of heat exchanger networks: from a thorough data extraction to robustness evaluation. Chem. Eng. Res. Des. 131, 571–583. https://doi.org/10.1016/j.cherd.2017.11.036.

Pintaric, Z., Kravanja, Z., 2015. A methodology for the synthesis of heat exchanger networks having large numbers of uncertain parameters. Energy 92, 373–382. https://doi.org/10.1016/j.energy.2015.02.106.

Ratnam, R., Patwardhan, V.S., 1991. Sensitivity analysis for heat exchanger networks. Chem. Eng. Sci. 46, 451–458. https://doi.org/10.1016/0009-2509(91)80006-K.

Ravagnani, M.A.S.S., Mano, T.B., Carvalho, E.P., Silva, A.P., Costa, C.B.B., 2014. Multi-objective Heat Exchanger Networks Synthesis Considering Economic and Environmental Optimization, in: Klemeš, J.J., Varbanov, P.S., Liew, P.Y. (Eds.), Computer Aided Chemical Engineering, 24 European Symposium on Computer Aided Process Engineering. Elsevier, pp. 1579–1584. https://doi.org/10.1016/B978-0-444-63455-9.50098-2.

Ryu, J., Kong, L., Pastore de Lima, A.E., Maravelias, C.T., 2020. A generalized superstructure-based framework for process synthesis. Comput. Chem. Eng. 133, 106653 https://doi.org/10.1016/j.compchemeng.2019.106653.

Shivakumar, K., Narasimhan, S., 2002. A robust and efficient NLP formulation using graph theoretic principles for synthesis of heat exchanger networks. Comput. Chem. Eng. 26, 1517–1532. https://doi.org/10.1016/S0098-1354(02)00089-3.

Sreepathi, B.K., Rangaiah, G.P., 2014. Improved heat exchanger network retrofitting using exchanger reassignment strategies and multi-objective optimization. Energy 67, 584–594. https://doi.org/10.1016/j.energy.2014.01.088.

Stampfli, J.A., Ong, B.H.Y., Olsen, D.G., Wellig, B., Hofmann, R., 2023. Multi-objective evolutionary optimization for multi-period heat exchanger network retrofit. Energy 281, 128175. https://doi.org/10.1016/j.energy.2023.128175.

Swaney, R., Grossmann, I., 1985a. An index for operational flexibility in chemical process design.1. formulation and theory. AIChE J 31, 621–630. https://doi.org/10.1002/aic.690310412.

Swaney, R., Grossmann, I., 1985b. An index for operational flexibility in chemical process design.2. computational algorithms. AIChE J 31, 631–641. https://doi.org/10.1002/aic.690310413.

Tarjan, R., 1971. Depth-first search and linear graph algorithms, in: 12th Annual Symposium on Switching and Automata Theory (Swat 1971). pp. 114–121. https://doi.org/10.1109/SWAT.1971.10.

Tian, Y., Li, S., 2023. Cost allocation evaluation of a multi-plant flexible heat exchanger network design based on fuzzy game. Comput. Chem. Eng. 175, 108262 https://doi.org/10.1016/j.compchemeng.2023.108262.

Toffolo, A., 2009b. The synthesis of cost optimal heat exchanger networks with unconstrained topology. Appl. Therm. Eng. 29, 3518–3528. https://doi.org/10.1016/j.applthermaleng.2009.06.009.

Toffolo, A., 2009. Multi-objective synthesis optimization of heat exchanger networks with arbitrary topology. Presented at the ASME 2008 International Mechanical Engineering Congress and Exposition, American Society of Mechanical Engineers Digital Collection, pp. 307–319. https://doi.org/10.1115/IMECE2008-68651.

Verheyen, W., Zhang, N., 2006. Design of flexible heat exchanger network for multi-period operation. Chem. Eng. Sci. 61, 7730–7753. https://doi.org/10.1016/j.ces.2006.08.043.

Wang, K., Qian, Y., Huang, Q., Yuan, Y., Yao, P., 1999. New model and new algorithm for optimal synthesis of large scale heat exchanger networks without stream splitting. Comput. Chem. Eng. S149–S152. https://doi.org/10.1016/S0098-1354(99)80037-4.

Warshall, S., 1962. A theorem on boolean matrices. Journal of the ACM (JACM). https://doi.org/10.1145/321105.321107.

Xu, Y., Zhang, L., Cui, G., Yang, Q., 2023. A heuristic approach to design a cost-effective and low-CO2 emission synthesis in a heat exchanger network with crude oil distillation units. Energy 271, 126972. https://doi.org/10.1016/j.energy.2023.126972.

Yan, L., 2004. Subgraphs of maximum matching graphs. Indian J. Pure Appl. Math. 35, 1063–1067.

Yang, Y.H., Gong, J.P., Huang, Y.L., 1996. A simplified system model for rapid evaluation of disturbance propagation through a heat exchanger network. Ind. Eng. Chem. Res. 35, 4550–4558. https://doi.org/10.1021/ie960321c.

Yang, Y., Zhang, L., Yuan, Y., Sun, J., Che, Z., Qiu, Z., Du, T., Na, H., Shuai, C., 2023. Muti-objective optimization on energy consumption, CO2 emission and production cost for iron and steel industry. J. Environ. Manage. 347, 119102 https://doi.org/10.1016/j.jenvman.2023.119102.

Yang, R., Zhuang, Y., Zhang, L., Du, J., Shen, S., 2020. A thermo-economic multi-objective optimization model for simultaneous synthesis of heat exchanger networks including compressors. Chem. Eng. Res. Des. 153, 120–135. https://doi.org/10.1016/j.cherd.2019.10.011.

Yee, T.F., Grossmann, I.E., Kravanja, Z., 1990. Simultaneous optimization models for heat integration—I. Area and energy targeting and modeling of multi-stream exchangers. Comput. Chem. Eng. 14, 1151–1164. https://doi.org/10.1016/0098-1354(90)85009-Y.

Zhang, D., Lv, D., Yin, C., Liu, G., 2020. Combined pinch and mathematical programming method for coupling integration of reactor and threshold heat exchanger network. Energy 205, 118070. https://doi.org/10.1016/j.energy.2020.118070.

Zhang, X.L., Yin, H.C., Huo, Z.Y., 2011. Flexible synthesis of heat exchanger network with particle swarm optimization algorithm. Adv. Mat. Res. 214, 569–572. https://doi.org/10.4028/www.scientific.net/AMR.214.569.

Zhao, L., Liu, G., 2022. Dynamic coupling of reactor and heat exchanger network considering catalyst deactivation. Energy 260, 125161. https://doi.org/10.1016/j.energy.2022.125161.

Zhao, L., Liu, G., 2023. Bottleneck-identification methodology and debottlenecking strategy for heat exchanger network with disturbance. Chem. Eng. Sci. 275, 118727 https://doi.org/10.1016/j.ces.2023.118727.

Zhu, J., Han, Z., Rao, M., Chuang, K., 1996. Identification of heat load loops and downstream paths in heat exchanger networks. Can. J. Chem. Eng. 74, 876–882. https://doi.org/10.1002/cjce.5450740609.

Zhu, Q., Zhang, B., Chen, Q., He, C., Foo, D.C.Y., Ren, J., Yu, H., 2020. Model reductions for multiscale stochastic optimization of cooling water system equipped with closed wet cooling towers. Chem. Eng. Sci. 224, 115773 https://doi.org/10.1016/j.ces.2020.115773.

Zirngast, K., Kravanja, Z., Pintaric, Z., 2021. An improved algorithm for synthesis of heat exchanger network with a large number of uncertain parameters. Energy 233, 121199. https://doi.org/10.1016/j.energy.2021.121199.